https://doi.org/10.5194/egusphere-2026-1615
Preprint. Discussion started: 8 April 2026

Assessment of Aerosol Iron Solubility using Global Dataset, Part II: Machine Learning and Deep Neural Network Coupled with SHapley Additive exPlanation Combined with Independent Component Analysis (SHAP-ICA)

Kohei Sakata[1], Minako Kurisu[2], Yoshio Takahashi[3]

[1]Materials Science and Engineering, Graduate School of Engineering, Tokyo Denki University, 5 Senjyu-Asahi-Cho, Adachi-ku, Tokyo 120-8551, Japan.

[2]Atmosphere and Ocean Research Institute, The University of Tokyo, 5-1-5, Kashiwanoha, Kashiwa, Chiba 277-8564, Japan.

[3]Graduate School of Science, The University of Tokyo, 7-3-1, Hongo Bunkyo-ku, Tokyo 113-0033, Japan.

Corresponding author: Kohei Sakata (kohei.sakata.33@mail.dendai.ac.jp)

Abstract.

The supply of dissolved iron (d-Fe) can enhance marine CO_2 fixation. Aerosols are one source of d-Fe to the ocean surface, but aerosol iron solubility (Fe_{sol}%) depends on emission sources and atmospheric alteration processes that remain poorly reproduced by global climate and chemical transport models. Although recent advances in machine and deep learning models can capture nonlinear relationships in observational datasets, applications to environmental samples are still limited and approaches for improving interpretability require further development. This study trained XGBoost and a deep neural network (DNN) using East Asian aerosol data and tested whether Fe_{sol}% and d-Fe concentrations in marine aerosols can be reproduced. The effects of individual features on Fe_{sol}% and d-Fe were quantified using SHapley Additive exPlanations (SHAP), and independent component analysis (ICA) was applied to SHAP values to extract independent components representing dominant controlling processes of Fe_{sol}%. East Asian Fe_{sol}% was reproduced well by both XGBoost and DNN. For marine aerosols, higher reproducibility was achieved by the DNN than by XGBoost, likely because deeper relationships among features can be learned. SHAP indicated that variability in Fe_{sol}% and d-Fe is primarily driven by chemical alteration of Fe in mineral dust and anthropogenic aerosols. ICA further suggested that additional processes, including heavy oil combustion, influence a subset of samples. Spatial variations in process contributions were visualized by mapping the influence of each independent component. This DNN-based framework can improve interpretation of both current results and future observational datasets.

https://doi.org/10.5194/egusphere-2026-1615
Preprint. Discussion started: 8 April 2026

1 Introduction

Iron (Fe), one of the most abundant metal elements in aerosol particles, plays diverse roles in atmospheric and environmental processes. These include supplying nutrients to surface seawater (Jickells et al., 2005; Mahowald et al., 2009, 2018), catalyzing sulfate aerosol formation via oxidation of sulfur dioxide (Alexander et al., 2009; Harris et al., 2013; Liu et al., 2021), facilitating methane removal through a photocatalytic chlorine atom cycle (Oeste et al., 2017; van Herpen et al., 2023; Meidan et al., 2024), and generating reactive oxygen species within the human body (Fang et al., 2017; Shiraiwa et al., 2017). Consequently, aerosol Fe is closely linked to socially relevant issues such as climate change and the health impacts of air pollution. Dissolved iron (d-Fe) plays a particularly important role in these processes, but aerosol Fe is mainly emitted as insoluble Fe (e.g., mineral dust). Therefore, the fractional solubility of aerosol Fe (Fe_{sol}%, defined as the ratio of d-Fe to total Fe) is considered a key factor controlling these effects (Jickells et al., 2005; Mahowald et al., 2009, 2018). From the perspective of Fe supply to the ocean, numerous observations, laboratory experiments, and modeling studies have investigated the factors controlling Fe_{sol}%. Nevertheless, substantial uncertainties remain (Baker et al., 2006; Buck et al., 2006, 2013; Sedwick et al., 2007; Olgun et al., 2011; Chance et al., 2015; Ito and Shi, 2016; Shelley et al., 2018; Conway et al., 2019; Kurisu et al., 2021, 2024; Sakata et al., 2022; Seo and Kim, 2023; Hsieh and Ho, 2024; Miyakawa et al., 2023; Ito and Miyakawa, 2023).

Most studies of Fe_{sol}% in marine aerosols have been conducted during research cruises (e.g., Baker et al., 2006; Buck et al., 2006, 2013; Chance et al., 2015; Kurisu et al., 2021, 2024; Sakata et al., 2022). However, each aerosol sample typically represents only one or two days within the target sea area or season, which will hereafter be referred to as the snapshot problem This makes it difficult to determine whether the samples collected are representative of the broader region or the sampling year (Mahowald et al., 2018). Long-term observations at fixed locations would help address the snapshot problem, but such observations are extremely challenging for marine aerosols. In Part I, we conducted a reanalysis using existing observational data. The results showed that monthly variations in Fe concentration and Fe_{sol}% in the North Pacific were similar to those observed in the East Asian region, a finding consistent with the strong influence of East Asian aerosol transport over this sea area. However, this alone cannot rule out the possibility that the similarities are coincidental.

One approach to assessing the representativeness of newly collected (unknown) samples is to build a regression model for Fe_{sol}% based on existing data. If the Fe_{sol}% of the unknown samples can be reproduced by such a model, it suggests that they follow the same functional relationships as previous observations, indicating a high likelihood of spatiotemporal representativeness. Conversely, model–observation mismatches may reveal controlling factors of Fe_{sol}% that are not included in the model. The behavior of Fe_{sol}% in aerosol particles is expected to follow a nonlinear function because it is influenced by multiple interacting factors, including atmospheric chemical alteration of Fe species and variations in Fe emission sources (Jickells et al., 2005; Mahowald et al., 2009, 2018). Previous studies have investigated individual factors, including anthropogenic Fe (anthro-Fe) contributions and aerosol acidity, using single-variable regression analyses; however, these approaches offer only limited understanding of the combined effects of multiple drivers. Modeling studies have also

https://doi.org/10.5194/egusphere-2026-1615
Preprint. Discussion started: 8 April 2026

attempted to predict Fe_{sol}%, but substantial parameter uncertainties remain, limiting predictive accuracy (Ito and Miyakawa, 2023; Hamilton et al., 2022; König et al., 2022).

In recent years, machine learning methods such as random forests, gradient boosting, and deep neural networks (DNNs) have advanced rapidly, with growing applications in atmospheric research (Gui et al., 2020; Shi et al., 2022; Li et al., 2022; Lin et al., 2022; Tao et al., 2022; Li et al., 2023; Peng et al., 2023). These methods can capture complex data structures beyond the scope of conventional statistical techniques and can produce more accurate regression models for target variables. However, they often suffer from the "black box" problem, making it difficult to interpret which features influence the predicted values. To address this issue, SHapley Additive exPlanations (SHAP) was employed (Lundberg and Lee, 2017). SHAP decomposes the predicted Fe_{sol}% of each sample into the mean predicted value and the summed contributions of all input features. In this framework, a SHAP value represents the contribution of a given feature to the deviation from the mean predicted value, which allows sample-specific contributions to be quantified. Mean absolute SHAP values further yield a global explanation of the model that is commonly interpreted as feature importance. In geochemistry and atmospheric chemistry, concentrations and concentration ratios are often selected as features. These variables are sensitive to specific processes, but they are not exclusively controlled by a single physical or chemical process. In addition, a single physical or chemical process can influence multiple features at the same time. SHAP provides feature-wise contributions, which makes it difficult to assign a given contribution to a single process when features are not process-specific in this strict sense. Consequently, emission sources and chemical reactions may appear in the covariation of multiple SHAP values rather than in any single SHAP value.

Covariation patterns are commonly analyzed using principal component analysis (PCA). PCA extracts orthogonal (uncorrelated) components along directions of maximum variance, but the resulting components do not guarantee statistical independence. Consequently, when multiple influences increase and decrease simultaneously and share variance, PCA tends to yield components that explain them collectively rather than separating them, and a single component may appear as a combination of multiple features. In contrast, independent component analysis (ICA) assumes that the observed multivariate data can be represented as a linear mixture of multiple components. ICA extracts mutually independent components by maximizing non-Gaussianity based on higher-order statistics (e.g., kurtosis). Thus, when such mixing is present, ICA has the potential to recover feature-contribution patterns in a more separated manner than PCA. Therefore, in this study, ICA was applied to SHAP values to isolate and extract the latent mechanisms driving the predictions for individual samples.

In this study, regression models were constructed using XGBoost and DNN combined with SHAP and ICA to reproduce Fe_{sol}% in East Asian aerosols and to evaluate the factors controlling Fe_{sol}% in aerosol particles. Regression models for d-Fe concentrations were also developed because substantial amounts of d-Fe can be supplied during mineral dust events even when Fe_{sol}% is low. To our knowledge, this study is the first to apply ICA to SHAP values in atmospheric chemistry, enabling the extraction of statistically independent source signals underlying model predictions. The overarching objectives of this work are therefore (1) to develop generalizable regression models for Fe_{sol}% and d-Fe that incorporate SHAP-ICA to

https://doi.org/10.5194/egusphere-2026-1615
Preprint. Discussion started: 8 April 2026

overcome the snapshot problem, and (2) to assess their applicability to aerosols in the North Pacific and other ocean basins that are strongly influenced by East Asian outflows, ultimately allowing a quantitative evaluation of the factors controlling Fe_{sol}%.

2. Methods

2.1 Input parameters

The same dataset as used in Part I was employed for XGBoost and DNN modeling. Total Fe (T-Fe) and total Al (T-Al) concentrations were determined by X-ray fluorescence analysis (XRF) or by inductively coupled plasma mass spectrometry (ICP-MS) and optical emission spectrometry (ICP-OES) after acid digestion using nitric and hydrofluoric acids. The concentrations of dissolved Fe (d-Fe) and dissolved Al (d-Al) were determined by ICP-MS or ICP-OES after extraction with ultrapure water or ammonium acetate (pH 4.7).

For constructing models using XGBoost and TensorFlow neural networks, the number of training samples is a critical factor affecting model performance. However, these models cannot handle samples with missing values. Therefore, features that are easy to obtain from a large number of samples are preferred. In this study, four features were selected to reproduce Fe_{sol}% and d-Fe concentration in aerosol particles (Table 1). Total Fe concentration (T-Fe) was used as an indicator of total Fe (including mineral dust and anthro-Fe). Fractional Al solubility (Al_{sol}% = d-Al/T-Al × 100) was used as an indicator of the degree of chemical alteration of mineral dust for XGBoost and DNN model reproducing Fe_{sol}%. In the case of d-Fe concentration reproduction, d-Al concentration was used as the indicator of the degree of chemical alteration of mineral dust.

The ratio of T-Fe to T-Al (T-Fe/T-Al) was used as an indicator of the source of Fe in aerosol particles. When mineral dust is dominated, the T-Fe/T-Al ratio is similar to that for the average upper continental crust (T-Fe/T-Al: 0.52 ± 0.12). In contrast, elevated T-Fe/T-Al ratios are observed when anthro-Fe is prominent, reflecting its occurrence mainly as hematite and magnetite nanoparticles (Kurisu et al., 2019; Li et al., 2021; Sakata et al., 2023). Thus, a higher T-Fe/T-Al ratio indicates a greater contribution of anthro-Fe to total Fe in aerosol particles. The [d-Fe]/[d-Al] ratio generally ranges from 0.2 to 0.5 when mineral dust dominates but becomes elevated when anthro-Fe oxide particles contribute to d-Fe. Anthro-Fe in aerosol particles can be either highly soluble upon emission or initially insoluble but subsequently solubilized through atmospheric chemical alterations (e.g., proton-promoted and ligand-promoted dissolution). Accordingly, the [d-Fe]/[d-Al] ratio is employed here as an indicator of both the contribution of anthro-Fe to d-Fe and the extent of its atmospheric processing.

https://doi.org/10.5194/egusphere-2026-1615
Preprint. Discussion started: 8 April 2026

125

Table 1. Input features for machine learning and deep learning of Fe_{sol}% and d-Fe concentration.

Features	Expected roles
T-Fe concentration	Total Fe loading in the atmosphere
Al solubility (Al_{sol}%)	Chemical alteration of mineral dust (only for Fe_{sol}%)
d-Al concentration	Chemical alteration of mineral dust (only for d-Fe concentration)
T-Fe/T-Al	Contribution of anthro-Fe to T-Fe
[d-Fe]/[d-Al]	Contribution of anthro-Fe to d-Fe and chemical alteration of anthro-Fe

These parameters were determined through feature optimization (i.e., feature engineering, see Supplemental Text S2 and Figure S1). At this time, multicollinearity is the state where a high correlation exists among features, preventing these correlated features from being treated as independent (Allin, 2010; Chan et al., 2022). When present, this condition can 130 compromise the reliability of model estimates and prediction power. Furthermore, the evaluation of feature importance by SHAP also assumes that features are independent. Therefore, the impact of multicollinearity must be mitigated as much as possible. In this study, we assessed the influence of multicollinearity using the correlation matrix and the variance inflation factor (VIF) between features (Allin, 2010; Chan et al., 2022). The correlation matrix evaluates the correlation among individual features as a means of detecting potential redundancy. VIF serves to quantify the magnitude of the collinearity's 135 influence on the overall stability and reliability of the model's parameter estimates. Mathematically, the VIF is calculated using the coefficient of determination (r^2) obtained from regressing a particular independent variable against all other independent variables. The formula for the VIF for feature *i* is:

$$VIF_i = \frac{1}{1-r_i^2} \quad \text{(Eq. 1)}$$

where r is the coefficient of determination of the multiple regression of feature *i* on all other features. VIF values below 5 140 indicate minimal multicollinearity impact; 5 to 10 suggests a moderate impact; and 10 or greater signals a severe problem.

2.2 Training and application dataset

While XGBoost can handle missing values, DNNs require that such data be either removed or imputed. In this study, imputation was not performed to prevent samples lacking actual concentration information from adversely affecting model accuracy. For a fair comparison between DNN and XGBoost, samples with missing values were also excluded. Four datasets 145 were constructed: East Asia (n: 428), North Pacific (n: 233), Atlantic Ocean (n: 361), and South Pacific (n: 73) (Figure 1).

https://doi.org/10.5194/egusphere-2026-1615
Preprint. Discussion started: 8 April 2026

These datasets included not only total suspended particulate (TSP) but also coarse and fine particles collected by size-fractionated sampling. The East Asian aerosol dataset was used to train XGBoost and DNN models to reproduce Fe_{sol}% and d-Fe concentrations, while the marine aerosol datasets served as application datasets to evaluate whether the models could reproduce Fe_{sol}%. Compared to marine aerosol datasets, the East Asian dataset encompasses a broader range of values for Fe_{sol}%, Al_{sol}%, T-Fe/T-Al, and [d-Fe]/[d-Al] (Figure 1). Nevertheless, it only partially covers the range of T-Fe, d-Fe, and d-Al concentrations. Specifically, samples with T-Fe below 1.0 ng/m³ are rarely observed in East Asian aerosols (Figure 1a), whereas such low-concentration samples are relatively common in marine aerosols (Figure 1b–1d). Furthermore, South Pacific aerosols include d-Fe and d-Al concentrations below 0.01 ng/m³ (Figure 1d), which are rarely observed elsewhere. When reproducing Fe_{sol}% for low-concentration samples, machine learning (XGBoost) and deep learning (DNN) models built using the East Asian aerosol training dataset must extrapolate the relevant concentration parameters. The present study investigates whether the models can accurately capture object values (Fe_{sol}% or d-Fe concentration) despite the several features needed for extrapolation.

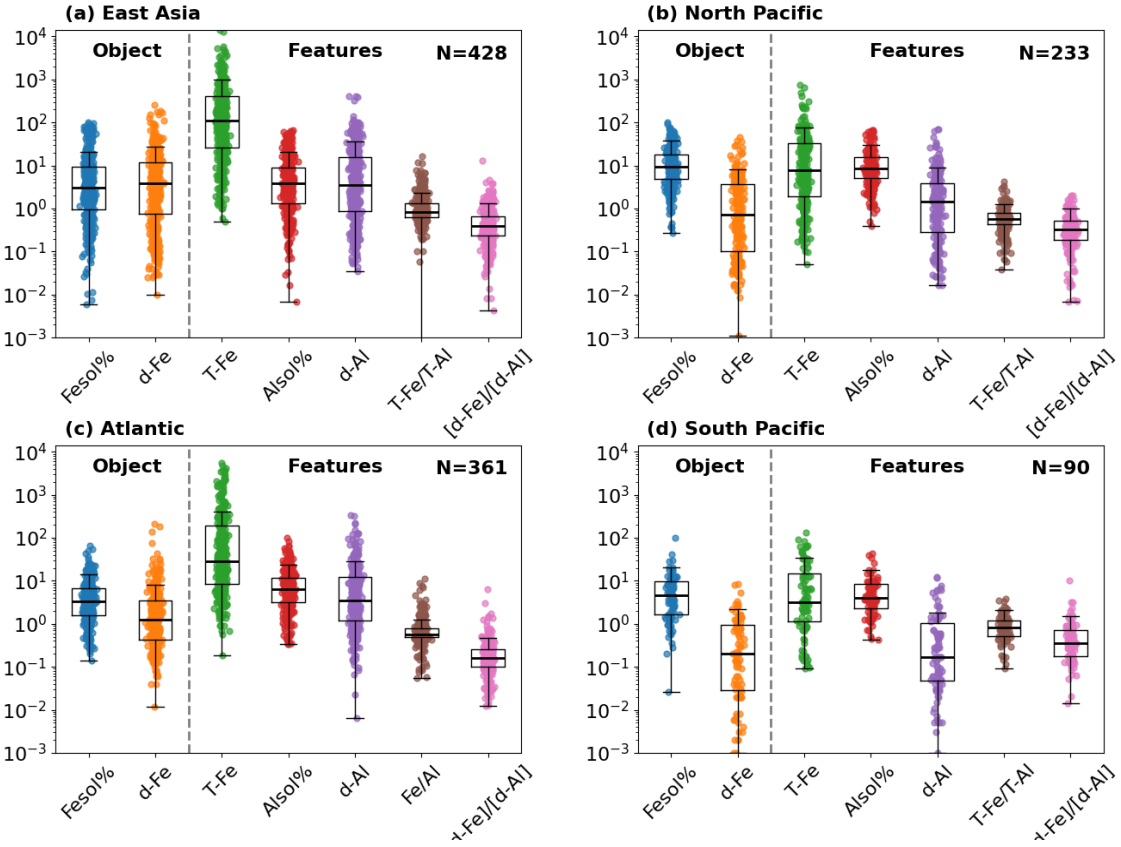

Figure 1. Scatter plot (colored plot) and box plots of object values and features in datasets of (a) East Asia, (b) North Pacific, (c) Atlantic, and (d) South Pacific. The box shows the 25th to 75th percentiles, with the median marked inside.

https://doi.org/10.5194/egusphere-2026-1615
Preprint. Discussion started: 8 April 2026

2.3 K-Fold cross validation and loss functions

For both XGBoost and DNN analyses, the East Asian sample dataset was randomly divided into training (80%) and testing (20%) subsets. The regression models were developed using the training subset, while the testing subset was reserved for independent model evaluation. To rigorously assess model performance and generalizability, K-fold cross-validation was employed (Figure S2). Specifically, the training data were further partitioned into five folds, and five regression models were iteratively trained, each time designating a distinct fold as the validation subset. Subsequently, the testing data were evaluated using these models, and the mean performance metrics across all models were reported. Model accuracy was quantified using the mean absolute error (MAE) and root mean squared error (RMSE), which were computed as follows:

$$MAE = \frac{\sum_{i=1}^{n}|y_i-\hat{y}_i|}{n}, \quad \text{(Eq. 2)}$$

$$RMSE = \sqrt{\frac{\sum_{i=1}^{n}(y_i-\hat{y}_i)^2}{n}}, \quad \text{(Eq. 3)}$$

where n is the numbers of sample, y_i is the observed value of sample i, ŷ is modeled value of sample i, and ȳ is the mean of samples.

2.4 Extreme Gradient Boosting Decision Tree

XGBoost analysis was performed separately on aerosol particles collected in East Asia, the North Pacific, the South Pacific, and the Atlantic Ocean. The model utilized the MAE as its loss function, and model training was conducted using five-fold cross-validation. The number of boosting rounds (i.e., number of iterations) was set at 500. Overfitting is a common issue in machine learning, in which a model fits the training data, including noise and random fluctuations, too closely and therefore shows poor generalization to unseen data such as validation and test sets. Early stopping was employed to prevent overfitting, halting the training process automatically if the model's performance on the validation set did not improve for 40 consecutive rounds. The tree depth, learning rate, subsample ratio (the fraction of training data sampled for each tree), and colsample_bytree ratio (the fraction of features sampled for each tree) were set to 3, 0.1, 0.8, and 0.8, respectively. These parameters were determined by grid search with holdout validation, while other parameters remained at their default settings. Feature importance for Fe_{sol}% across these regions was evaluated using SHAP, as described in Section 2.7. Moreover, to assess the influence of East Asian aerosols on North Pacific aerosols, a regression model trained on East Asian aerosols was applied to all North Pacific aerosols as test data.

https://doi.org/10.5194/egusphere-2026-1615
Preprint. Discussion started: 8 April 2026

2.5 Deep neural network

DNN model was constructed using the Keras library with TensorFlow (version 2.12.0). The DNN architecture comprised an input layer with 4 nodes, three hidden layers (the first two with 64 nodes each and the third with 32 nodes), and an output layer with one node (Figure S3a). All layers were fully connected (dense) to the next layer. The rectified linear unit (ReLU; $f(x)$=max(0,x)) was used as the activation function (Figure S3b). Adam optimizer with a learning rate of 0.001 and MAE as the loss function were employed. All input features were standardized to zero mean and unit variance prior to training. Model training was performed with a fixed random seed for reproducibility. Dataset of East Asian aerosol samples were split into training (80%) and validation (20%) sets. The DNN model training was carried out using 5-fold cross validation with 2000 epochs on the training dataset. Unlike XGBoost, early stopping was not employed for the DNN models. Instead, for each training fold, the model corresponding to the epoch with the minimum MAE was selected as optimal. These procedures were implemented to mitigate overfitting in the DNN. Similarly to XGBoost, SHAP analysis and regression analysis of Fe_{sol}% in marine aerosols using the model trained on East Asian aerosols were performed.

2.6 Shapley Additive explanation (SHAP)

SHAP was utilized to obtain both local and global interpretability of the model. Conceptually, SHAP considers all possible coalitions of features and evaluates how the model prediction changes when a given feature is added to or removed from these coalitions. At the local level, SHAP values explain individual predictions; by aggregating these local explanations over all samples (e.g., via the mean absolute SHAP value), a global view of feature importance is obtained relative to the mean modeled value $E[f(x)]$. A key advantage of SHAP is that it provides feature attributions for each individual sample, from which global feature importance metrics can be derived.

The SHAP value quantifies the contribution of feature to the overall outcome of a cooperative game. It is defined as the expected marginal contribution of feature across all possible orders in which the features can enter a coalition. Mathematically, SHAP values for feature i is expressed as:

$$\phi_i = \sum_{S \subseteq N \setminus \{i\}} \frac{|S|!(|F|-|S|-1)!}{|F|!} [f_x(S \cup \{i\}) - f_x(S)] \quad \text{(Eq. 4)}$$

where $F$is the set of all features and the summation is taken over all subsets $S$of Fthat do not contain feature i. The term of $\frac{|S|!(|F|-|S|-1)!}{|F|!}$ is the weight assigned to coalition S, corresponding to the probability that the features in Sappear before feature $i$in a random ordering of all features. The term $[f_x(S \cup \{i\}) - f_x(S)]$ represents the marginal contribution of feature $i$to coalition S, i.e., the change in the value function $f_x$when feature $i$is added to S. Thus, the Shapley value aggregates these marginal contributions, weighted by the likelihood of each coalition formation order. Since SHAP belongs to the class of

https://doi.org/10.5194/egusphere-2026-1615
Preprint. Discussion started: 8 April 2026

additive feature attribution methods, the model prediction $f(x_i)$ for any sample i can be decomposed into the baseline prediction $E[f(x)]$ and the SHAP values $\phi_j(x_i)$ for each feature j:

$$f(x_i) = E[f(x)] + \sum_{j=1}^{M} \phi_j(x_i) \quad \text{(Eq. 5)}$$

Consequently, SHAP values have the same units as the target variable (e.g., % for Fe_{sol}% and ng m^{-3} for d-Fe concentration). Here, $\phi_j(x_i)$ represents the contribution of feature j for sample i: a positive value indicates that the feature increases the prediction relative to the mean prediction, whereas a negative value indicates that it decreases the prediction. Because SHAP values are defined as changes relative to the mean prediction and are computed while accounting for feature interactions, they can sometimes take seemingly implausible negative values or, when considered in isolation, absolute values that lie outside the physically meaningful range of the target variable (e.g., 0–100% for Fe_{sol}%). However, the SHAP values for all features are constrained to sum exactly to the model prediction $f(x_i)$, so positive and negative contributions are balanced across features in a relative manner. Therefore, SHAP values can be interpreted as indicating how much each feature pushes the model prediction above or below the mean, and the magnitude of their absolute values can be appropriately used as a measure of the strength of each feature's contribution.

Finally, to obtain a global explanation of feature importance for Fe_{sol}% over the entire dataset, the mean absolute SHAP value for each feature was calculated.

2.8 Independent component analysis of SHAP values of each feature

The features used in this study were chosen because they are most sensitive to specific physical or chemical processes, although they can also be affected by other processes (e.g., an increase in anthro-Fe concentration can simultaneously enhance both T-Fe and T-Fe/T-Al). Thus, the observed values of each feature represent a superposition of multiple processes and are used as tracers of the process expected to be dominant. Covariation patterns in the SHAP values of these features (i.e., the simultaneous response of all four features to a given process) were assumed to reflect the influence of individual physical and chemical processes on the features themselves and on Fe_{sol}% and d-Fe concentrations. To extract such patterns, independent component analysis (ICA) was applied to the matrix composed of SHAP value vectors for the four input features for each sample *i*. ICA assumes that multivariate data can be represented as a linear combination of statistically independent components and yields independent components together with the contribution of each feature to each component. In this study, each component was interpreted as a single physical or chemical process influencing Fe_{sol}% and d-Fe concentrations.

Practically, the SHAP values of each feature were first standardized to zero mean and unit variance, and the FastICA algorithm was then applied to the standardized matrix. Standardization was performed to prevent differences in

https://doi.org/10.5194/egusphere-2026-1615
Preprint. Discussion started: 8 April 2026

variance among features from dominating the estimation of independent components and to emphasize relative covariation patterns among features. The number of components was fixed at 4, equal to the number of input features. The physical and chemical processes represented by each component were inferred from the feature loading patterns, and the influence of each component on Fe_{sol}% and d-Fe concentrations was evaluated from the relationships between the component scores (for each sample) and Fe_{sol}% and d-Fe.

3 Results and Discussion

3.1 Model performances of XGBoost and DNN

Figure 3 compares the performance of the XGBoost and DNN models, which were optimized to reproduce Fe_{sol}% and d-Fe concentrations in East Asian aerosols. Both models showed good reproducibility over the wide dynamic range spanning four orders of magnitude present in the East Asian dataset (Figure 2). Furthermore, the small variability in reproduced values during 5-fold cross-validation (Figures S4 and S5) indicates the high stability of both models. This implies that the models are reliably capturing the underlying patterns of the entire dataset, rather than overfitting them to specific training subsets.

Comparing the reproduction accuracy for Fe_{sol}% and d-Fe concentration between XGBoost and DNN, the DNN showed higher reproducibility because DNN showed lower MAE and RMSE than those for XGBoost (Figure 3). This performance difference is primarily attributed to the degraded reproducibility of XGBoost in the region where Fe_{sol}% and d-Fe concentrations are lower than 0.2% and 0.2 ng m^{-3}, respectively (Figure 2). This is likely due to the limited number of such samples in the East Asian dataset (Figure 1a). The differences in stability in the low Fe_{sol}% and d-Fe concentration regions were attributed to the algorithmic characteristics of both models. XGBoost, as a decision-tree-based method, learns by splitting the feature space. In data-sparse regions, it lacks sufficient samples to define optimal splits, causing minor training data fluctuations to significantly alter the model structure and increase the variance of its reproductions. Conversely, a DNN learns a continuous non-linear function, enabling it to interpolate effectively in sparse regions using information from denser regions.

https://doi.org/10.5194/egusphere-2026-1615
Preprint. Discussion started: 8 April 2026

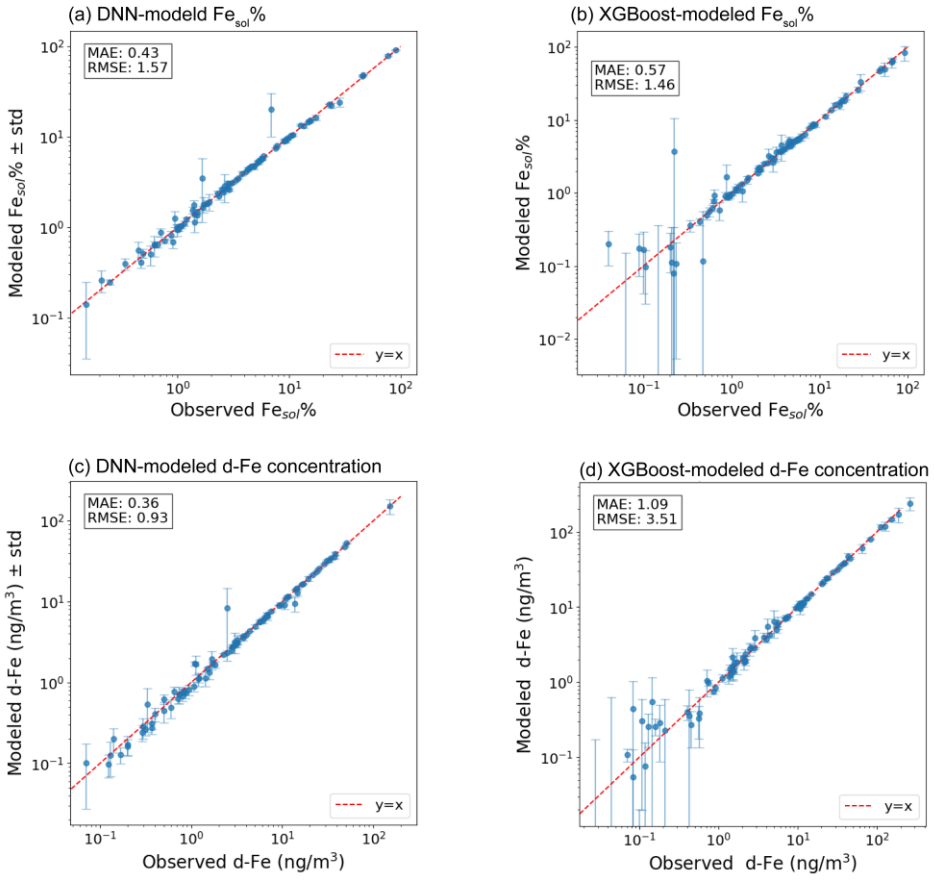

Figure 2. Scatter plots showing observed versus modeled values of Fe_{sol}% for (a) DNN and (b) XGBoost, and d-Fe concentration for (c) DNN and (d) XGBoost.

3.2 Evaluation of feature importances using SHAP and ICA

3.2.1 SHAP

Figure 3 shows SHAP values for each feature obtained from XGBoost and DNN models. The features are plotted from top to bottom in descending order of the mean absolute SHAP value, where the point color indicates the magnitude of the corresponding feature value (in the case of Al_{sol}%, blue points represent lower Al_{sol}% and red points represent higher Al_{sol}%).

https://doi.org/10.5194/egusphere-2026-1615
Preprint. Discussion started: 8 April 2026

SHAP values represent the contribution of each feature defined relative to the mean model prediction across all samples, *E[f(x)]*, and they have the same units as the target variable (Fe_{sol}%: %; d-Fe concentration: ng m^{-3}). In other words, SHAP values quantify how much, and in which direction, each feature shifts the prediction for a given sample from this baseline to the final predicted value (Figures 3 and S6). Figure 3 shows feature-wise SHAP values computed for the trained XGBoost and DNN models. Features ranked higher in the upper panel have larger mean absolute SHAP values. In this study, both models reproduced the observed Fe_{sol}% and d-Fe concentrations well (Figure 3). Therefore, the SHAP values for each feature can be regarded as a quantitative indicator of how each process influences observations.

The most characteristic result obtained from the SHAP analysis of East Asian aerosols is that the SHAP values associated with T-Fe/T-Al decreased with increasing the ratio (Figure 3). This behavior indicated that a larger contribution of anthro-Fe leads to lower Fe_{sol}% in East Asian aerosols, meaning that anthro-Fe appears to be emitted predominantly in an insoluble form. Indeed, both the XGBoost and DNN models show that d-Fe concentrations respond only weakly to changes in T-Fe/T-Al. As discussed in detail in the sections on the model analysis for coarse and fine aerosol particles (Sections 3.3.1 and 3.3.2, respectively), recent studies have reported that anthro-Fe in East Asia mainly originates from Fe-oxide nanoparticles emitted by the steel industry and from brake-pad wear of vehicles, and that their Fe_{sol}% is often below 0.1% (Figures 4b and 4d). Consequently, simply increasing the atmospheric loading of anthro-Fe cannot enhance Fe_{sol}% in East Asian aerosols. In other words, the influence was limited for anthro-Fe sources that exhibit high Fe_{sol}% at the time of emission, such as heavy-oil combustion and gasoline combustion (Fe_{sol}% > 38%; Schroth et al., 2009; Oakes et al., 2012).

By contrast, the SHAP analysis shows that Al_{sol}% (degree of alteration of mineral dust), followed by [d-Fe]/[d-Al] (degree of alteration of anthro-Fe), indicated the largest influence on Fe_{sol}%. For both parameters, the SHAP value increased as their values increased (Figures 3a and 3c). Similar behavior was obtained from the model for reproducing d-Fe concentrations (Figures 3b and 3d), clearly demonstrating that chemical alterations of Fe-bearing particles during atmospheric transport are crucial for enhancing both Fe_{sol}% and d-Fe concentration. For Fe_{sol}%, the effects of the chemical alterations of mineral dust and anthro-Fe were comparable (Figures 3a and 3c), whereas in the case of d-Fe concentration, the importance of chemical alteration of mineral dust was clearly greater than that of anthro-Fe alteration (Figures 4b and 4d). This difference arises from the nature of the target variables. When Fe_{sol}% is used as the target, the model effectively learns the degree of alteration of Fe-bearing particles. As discussed in Part I, the Fe_{sol}% values of mineral dust and anthro-Fe in East Asian TSP differ only slightly, with mineral dust at 4.7 ± 4.5% and anthro-Fe at 1.7 ± 4.1%. Therefore, it is not surprising that the impacts of Al_{sol}% and [d-Fe]/[d-Al] on Fe_{sol}% did not differ greatly. In contrast, the contribution of anthro-Fe to d-Fe in East Asian TSP was on average only about 6.0% (see part I). In this case, explaining aerosol d-Fe concentrations necessarily requires a stronger influence from the mineral-dust alteration process than from anthro-Fe processes. As a result, a clear difference in the SHAP values for mineral dust and anthro-Fe emerges in the d-Fe model.

https://doi.org/10.5194/egusphere-2026-1615
Preprint. Discussion started: 8 April 2026

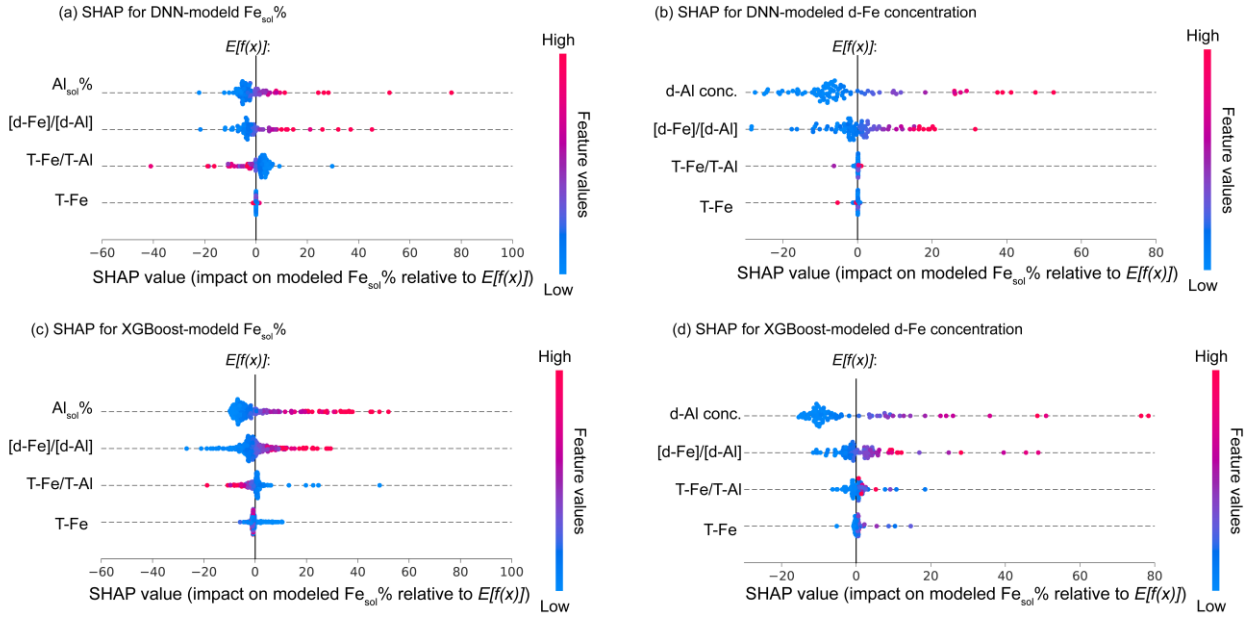

Figure 3. SHAP values for each feature impacting the (a and b) DNN-modeled Fe_{sol}% and d-Fe concentration, and (c and d) XGBoost-modeled Fe_{sol}% and d-Fe concentration. Features on the y-axis are ordered from top to bottom by their mean absolute SHAP value (average impact on the prediction). The x-axis shows the SHAP value for each individual sample, representing the deviation from the mean prediction (*E[f(x)]*, SHAP=0) attributed to that feature. Positive values indicate a contribution that increases the prediction, while negative values indicate a contribution that decreases it. The color of each point corresponds to the magnitude of the feature value (red: high, blue: low). For instance, in (a), the most influential feature (Al_{sol}%) shows that higher feature values (red points) correspond to positive SHAP values, indicating a strong positive contribution to the Fe_{sol}% prediction. (Results for the training dataset are shown in Figure S6.)

3.3.2 The processes controlling Fe_{sol}% identified by ICA

The matrix of SHAP values (features × samples) was subjected to ICA to infer independent physical and chemical processes. Figure 4 shows the loadings of each feature for the processes extracted as independent components (ICs) and relationship between IC score and observed Fe_{sol}%. For IC1, Al_{sol}% and the [d-Fe]/[d-Al] ratio associated with chemical alteration degree of Fe-bearing particles exhibited large positive loadings, whereas the loadings of T-Fe concentration and T-Fe/T-Al for mineral dust and anthro-Fe emissions were almost 0 (Figure 4a). Consequently, IC1 represented chemical alterations of mineral dust and anthro-Fe in the atmosphere were the dominant factor controlling Fe_{sol}% of East Asian aerosols. The scores of IC1 exhibit a strong positive correlation with the observed Fe_{sol}% (Figure 4a). Given that the

https://doi.org/10.5194/egusphere-2026-1615
Preprint. Discussion started: 8 April 2026

correlation coefficient between the score of this IC and Fe_{sol}% was the highest among all components, the physical and chemical processes represented by IC1 was the most important in controlling Fe_{sol}% in East Asian aerosols.

IC2 was characterized by a large positive loading for the T-Fe/T-Al ratio (Figure 4b), indicating that IC2 reflected the atmospheric loading of anthro-Fe characterized by high T-Fe/T-Al. Al_{sol}% and [d-Fe]/[d-Al] also had positive loadings, suggesting contributions to higher Fe_{sol}%. Given that the chemical alteration of anthro-Fe was already extracted as IC1, IC2 likely represents direct emissions of anthro-Fe that inherently have high Fe_{sol}% at the time of release. Consistently, higher IC2 scores tended to coincide with Fe_{sol}% exceeding 50%. However, samples with high IC2 scores accounted for only a small fraction of the dataset, and IC2 scores for most samples clustered near zero. These results suggest that direct emissions of high Fe_{sol}% anthro-Fe exert only a limited influence on Fe_{sol}% in East Asian aerosols.

The strong T-Fe loading indicates that IC3 represents a process that elevates atmospheric T-Fe concentrations (Figure 4c). Given that both T-Fe/T-Al and [d-Fe]/[d-Al] loaded negatively, the decrease in these ratios was likely driven by a larger mineral dust contribution to T-Fe and d-Fe (i.e., a reduced relative contribution from anthro-Fe). In contrast, Al_{sol}% showed little loading in IC3 (Figure 4c), suggesting that mineral dust did not undergo pronounced atmospheric alteration. Taken together, IC3 is consistent with mineral dust (dust-event) conditions, yet the lack of a clear relationship between IC3 and Fe_{sol}% indicated that this component was not major factor controlling Fe_{sol}% in East Asian aerosols. IC4 showed positive loadings of [d-Fe]/[d-Al] and T-Fe/T-Al, implying that this component reflects process associated with anthro-Fe (Figure 4d). However, IC3 and IC4 did not correlate with Fe_{sol}%, suggesting that these components may partly reflect noise in the ICA analysis.

https://doi.org/10.5194/egusphere-2026-1615
Preprint. Discussion started: 8 April 2026

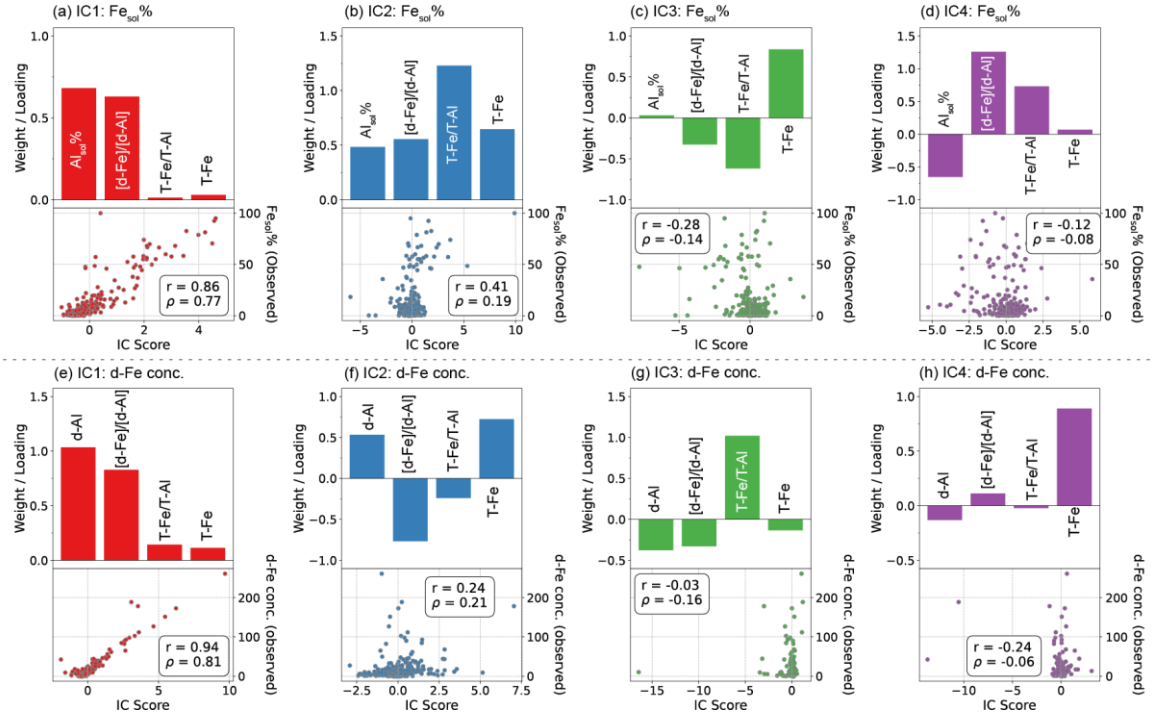

Figure 4. Feature loadings for each independent component (top panels) and scatter plots of IC scores versus Fe_{sol}% (bottom panels): (a) IC1, (b) IC2, (c) IC3, and (d) IC4. The ρ values in the bottom panels indicate Spearman's rank correlation coefficients.

3.3.3 The process controlling d-Fe concentration identified by ICA

ICA was also applied to the SHAP values for d-Fe (Figures 4e–h). In IC1, d-Al and [d-Fe]/[d-Al] showed strong positive loadings, whereas the contributions of T-Fe/T-Al and T-Fe were small and its IC scores were clearly correlated with d-Fe concentrations (Figure 4e). These results indicated that simply increasing the atmospheric inputs of mineral dust and anthro-Fe did not necessarily increase d-Fe concentration in East Asian aerosols. Thus, chemical alterations of mineral dust and anthro-Fe in the atmosphere is the dominant factor controlling d-Fe concentration in East Asian aerosols.

In IC2, d-Al and T-Fe had positive loadings, while T-Fe/T-Al and [d-Fe]/[d-Al] ratios had negative loadings (Figure 4f). This result suggested that IC2 reflected conditions under which T-Fe increases, such as mineral dust events. Although chemical alteration of mineral dust events were suggested to have little impact on Fe_{sol}% (Figure 4c), d-Al concentration also loaded positively in IC2. This likely reflected concurrent increases in the absolute supply of d-Al and d-Fe driven by

https://doi.org/10.5194/egusphere-2026-1615
Preprint. Discussion started: 8 April 2026

enhanced T-Fe inputs, even when Fe_{sol}% is low. However, because IC2 scores did not correlate with d-Fe concentrations, the influence of mineral dust events on the d-Fe budget over East Asia appears to be limited.

In IC3 and IC4, T-Fe/T-Al and T-Fe, respectively, showed positive loadings, but their scores clustered near zero, indicating a negligible influence on East Asian aerosols. Overall, these results suggest that chemical processing in the atmosphere controls both Fe_{sol}% and d-Fe concentrations over East Asia.

3.4 Size-dependences of SHAP-ICA results(ここから見直す)

Our SHAP-ICA results showed that the chemical alterations of mineral dust and anthro-Fe contributed to increases in Fe_{sol}% and d-Fe concentrations in East Asian aerosols (Figures 3 and 4), whereas the contribution of anthro-Fe to total Fe was associated with a decrease in Fe_{sol}% (Figure 3). This seems to contradict the common assumption that anthro-Fe from high-temperature combustion has higher Fe_{sol}% than mineral dust and is mainly present in fine aerosol particles. However, we compiled a single dataset by combining aerosol samples from the TSP, coarse, and fine fractions, but the mean Fe_{sol}% values for the coarse and TSP fractions (e.g., 1.0 ± 1.0% for coarse and 3.5 ± 3.2% for TSP) were approximately one order of magnitude lower than that for the fine fraction (21.0 ± 23.6%). As a result, coarse and TSP samples with high T-Fe/T-Al but low Fe_{sol}% can offset the influence of combustion-derived anthro-Fe in fine aerosol particles with both T-Fe/T-Al and Fe_{sol}% are high, leading to the apparent negative relationship between T-Fe/T-Al and Fe_{sol}%. To test this interpretation, we separately built DNN models for coarse and fine particles and evaluated the factors controlling Fe_{sol}% in each size fraction.

3.4.1 Coarse aerosol particles

DNN model well reproduced Fe_{sol}% in coarse aerosol particles (Figure S7a). SHAP analysis of the DNN model for coarse aerosol particles showed that the chemical alterations of mineral dust and anthro-Fe were the most important factors for Fe_{sol}%, whereas T-Fe/T-Al had a negative effect on Fe_{sol}% and T-Fe concentration has almost no effect (Figure 5a). These results suggested that mineral dust and anthro-Fe are emitted into the atmosphere mainly in insoluble Fe and they were converted to d-Fe through dissolution during atmospheric transport. It is noteworthy that, for coarse aerosol particles, the range of SHAP values is very narrow and the expected model output $E[f(x)]$ was as low as 2.1% (Figure 5a), indicating that the Fe_{sol}% in the coarse aerosol particles were less influenced by chemical alterations and contributions of anthro-Fe.

Based on the ICA results of the SHAP values, the processes that primarily affected Fe_{sol}% in coarse aerosol particles were captured by IC1 and IC2 (Figures 5 and 5c). The remaining components, IC3 and IC4, were interpreted as residual terms rather than physically meaningful processes due to the clustering of their scores near zero and the lack of any clear

https://doi.org/10.5194/egusphere-2026-1615
Preprint. Discussion started: 8 April 2026

correlation with observed Fe_{sol}% (Figure S7). IC1 has positive loadings for T-Fe/T-Al and Al_{sol}% (Figure 6b). As noted above, T-Fe/T-Al represents the contribution of anthro-Fe to total Fe. However, the lack of positive loading for [d-Fe]/[d-Al] suggested that anthro-Fe did not contribute to increases in Fe_{sol}%. This result implied that anthro-Fe present in coarse aerosol particles was insoluble form, consistent with result that the SHAP value decreased with increasing T-Fe/T-Al. One of the potential sources of Anthro-Fe with low Fe_{sol}% is non-exhaust vehicle (NEV) particles, including brake pads and tire wear debris in road dust. These materials were mainly composed of Fe-oxides, of which Fe_{sol}% is typically less than 0.1% (Shupert et al., 2013; Halle et al., 2021; Cui et al., 2025). In contrast, the positive loading of Al_{sol}% in IC1 indicated that chemical alteration of mineral dust contributed to enhance Fe_{sol}%. Mineral dust is known to be a major constituent of road dust; therefore, it is reasonable that this factor reflects contributions from mineral particles. Although the IC1 score correlated with Fe_{sol}%, the response was weak, and most Fe_{sol}% values were below 5% (Figure 5b). This result suggested that mineral dust is likely undergoing chemical alterations of Fe-bearing particles in coarse aerosol particles under weakly acidic conditions. This interpretation is also consistent with the contrasting solubilities of mineral particles and Anthro-Fe, because aluminosilicates generally exhibit higher solubility than Fe-oxides in weakly acidic solutions (Journet et al., 2007). Accordingly, IC1 represented the atmospheric emission of mineral particles and anthropogenic iron from road dust and their subsequent weathering processes.

[d-Fe]/[d-Al] and T-Fe/T-Al in IC2 had large loadings, whereas the contributions of the other features were negligible (Figure 5c). This pattern was interpreted as reflecting either processes that promote the solubilization of anthro-Fe in coarse aerosol particles or the direct emission of highly soluble anthro-Fe into the coarse fraction. However, IC2 scores clustered near zero for most samples, and only a small subset exhibited high IC2 scores together with high Fe_{sol}% (Figure 5c). These results suggest that the contribution of anthro-Fe to Fe_{sol}% in coarse particles is limited. In the case of IC3 and IC4, these IC scores wert not show any relationship with Fe_{sol}% (Figure S7b and S7c). Therefore, these ICs mainly capture residuals, noise, or secondary variability with little influence on Fe_{sol}%.

https://doi.org/10.5194/egusphere-2026-1615
Preprint. Discussion started: 8 April 2026

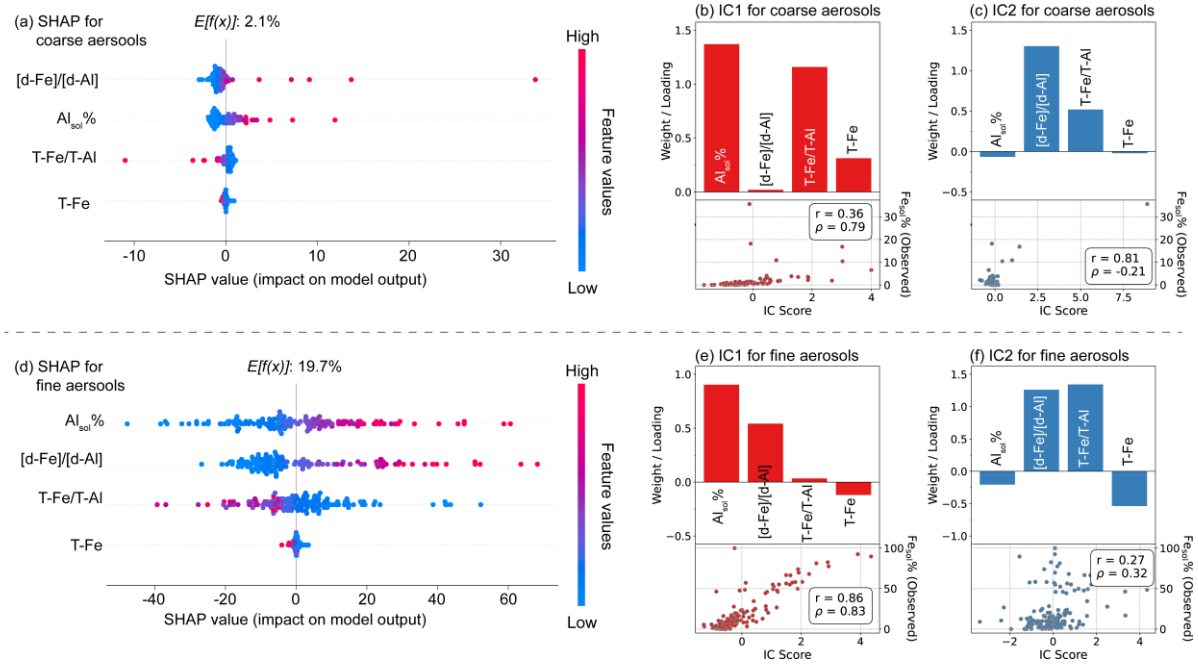

Figure 5. (a) SHAP values of each feature obtained from DNN model for coarse aerosol particles. Feature loadings for each independent component (top panels) and scatter plots of IC scores versus Fe_{sol}% (bottom panels): (b) IC1 and (c) IC2. (d-f) same for fine aerosol particles.

3.4.2 Fine aerosol particles

DNN model also well reproduced Fe_{sol}% in fine aerosol particles (Figure S7d). The chemical alterations of mineral dust and anthro-Fe were the dominant contributors of Fe_{sol}% in fine aerosol particles, of which SHAP values increase with increasing their value (Figure 5d). The SHAP values for these features spanned a broad range in both positive and negative directions (Figure 5d). This result indicated that Fe in fine aerosol particles was strongly solubilized by atmospheric chemical reactions (SHAP > 0), as well as samples that underwent only weak chemical alteration or almost no alteration (SHAP < 0). Even for fine aerosol particles that are strongly influenced by anthro-Fe emitted from high-temperature combustions (Kurisu et al., 2016, 2019), the SHAP value associated with the T-Fe/T-Al ratio decreased as this ratio increased (Figure 6d). This suggested that anthro-Fe in fine aerosol particles was also emitted into the atmosphere primarily as insoluble Fe, rather than as fly ash from heavy oil or gasoline combustion with high Fe_{sol}%. Recent studies have reported that anthro-Fe in fine aerosol particles (mainly $PM_{2.5}$) over East Asia originated from steel industry and NEV particles, of which Fe_{sol}% were typically low (Kajino et al., 2020; Ito et al., 2021; Cui et al., 2025; Kurisu et al., 2026). Therefore, simply increasing the atmospheric loading of anthro-Fe did not lead to an increase in Fe_{sol}% in fine aerosol particles is reasonable.

https://doi.org/10.5194/egusphere-2026-1615
Preprint. Discussion started: 8 April 2026

Similar to the coarse fraction, Fe_{sol}% in the fine fraction was mainly governed by two ICs (Figures 5e and 5f). The other two ICs were interpreted as noise-like or residual components (Figures S7e and S7f). IC1 showed large loadings of Al_{sol}% and [d-Fe]/[d-Al], whereas the loadings of T-Fe/T-Al and T-Fe were almost negligible (Figure 5e). This result indicated that IC1 reflected chemical alterations of both mineral dust and anthro-Fe that enhanced Fe_{sol}%, whereas the relative contribution of anthro-Fe to T-Fe was not a driver of higher Fe_{sol}%. In addition, a strong positive correlation was observed between the IC1 score and Fe_{sol}%. Thus, Fe_{sol}% in fine aerosol particles did not become high unless chemical alterations proceeded for both mineral dust and anthro-Fe. A similar independent component was also identified in the dataset constructed from all aerosol samples collected over East Asia. These findings suggested that, in East Asian aerosols, the chemical alterations of Fe in fine aerosol particles during atmospheric transport is the most important controlling factor governing Fe_{sol}%.

The [d-Fe]/[d-Al] and T-Fe/T-Al ratio in IC2 had positive loadings, whereas Al_{sol}% and T-Fe concentration had slightly negative loadings (Figure 5f). This pattern suggested that anthro-Fe strongly influences both T-Fe and d-Fe. Therefore, IC2 is interpreted as representing emissions of fly ash from heavy oil and gasoline combustion, in which both T-Fe and d-Fe are already high at the time of emission. Although some samples exhibited both high IC2 scores and high Fe_{sol}%, there was no clear correlation between them. This indicates that the variability of Fe_{sol}% in fine aerosol particles over East Asia cannot be adequately explained solely by the influence of anthro-Fe sources with high Fe_{sol}%.

3.5 Model performance across ocean basins

3.5.1 North Pacific aerosols

Mineral dust and anthro-Fe transported over East Asia are strongly affected by anthropogenic acid processing, which substantially enhances Fe_{sol}% (Liu et al., 2022; Shi et al., 2022; Sakata et al., 2022, 2023, 2025; Seo and Kim, 2023; Hsieh et al., 2022, 2023). This process is likely a major control on the Fe_{sol}% of North Pacific aerosols influenced by East Asian outflow (Buck et al., 2013; Sakata et al., 2022, 2025). To test this, we evaluated whether models trained on East Asian aerosols (EA-XGBoost and EA-DNN) could reproduce Fe_{sol}% in North Pacific aerosols.

The EA-DNN model reproduced both Fe_{sol}% and d-Fe concentration well in North Pacific aerosols (Figures 6a, 6b, S8b, and S9b), whereas the EA-XGBoost model performed much less well (Figures 6c, 6d, S8a, and S9a). This difference likely arises because XGBoost relies more heavily on pre-defined features, making it less transferable beyond the East Asian training domain, while the DNN can learn more generalizable feature representations during training. These results suggest that the EA-DNN model is more suitable for estimating Fe_{sol}% in marine aerosols, and only the EA-DNN results are therefore discussed below.

https://doi.org/10.5194/egusphere-2026-1615
Preprint. Discussion started: 8 April 2026

The EA-DNN model successfully reproduced Fe_{sol}% and d-Fe concentration in a large proportion of North Pacific aerosol samples collected during both winter–spring and summer–autumn (Figures 6a and 6b). Reproducibility was higher in winter–spring, when East Asian outflow to the North Pacific is strongest, indicating that many North Pacific aerosols were governed by processes similar to those controlling Fe_{sol}% in East Asia. In East Asian aerosols, poor reproducibility was mainly limited to samples with Fe_{sol}% below 1.0%, whereas in North Pacific aerosols it was mainly observed in summer–autumn samples with Fe_{sol}% above 10%. This difference likely reflects additional d-Fe sources or Fe dissolution processes that are absent in East Asia or far less prominent there, such as marine chemical alteration. The model also performed well for samples with d-Fe concentrations above 0.1 ng m^{-3}, but less well below this threshold, likely because such low-d-Fe cases were underrepresented in the East Asian training dataset.

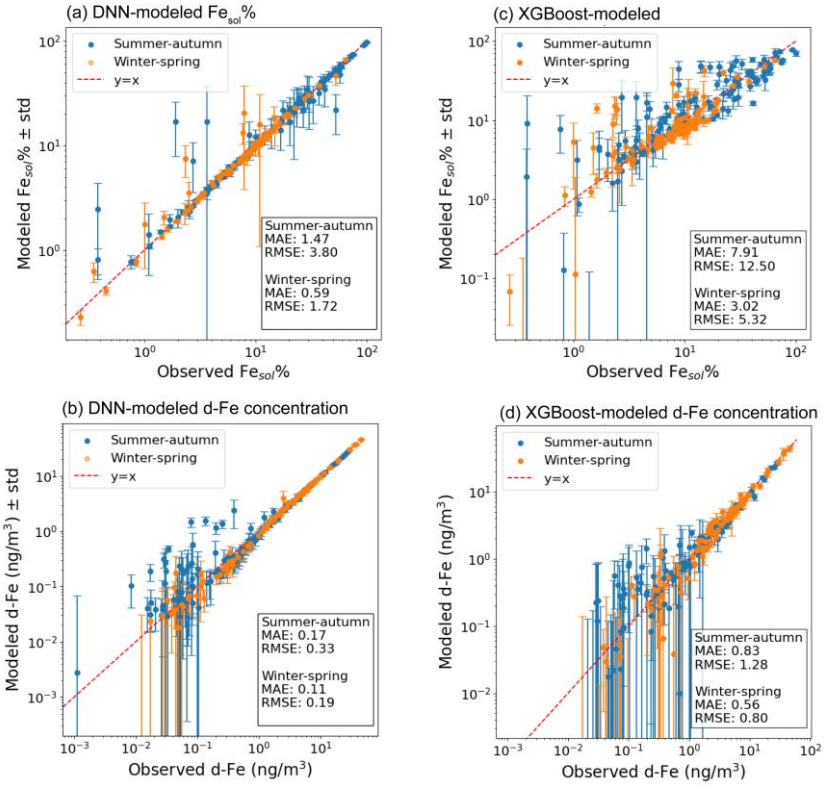

Figure 6. Accuracy and precision estimates for EA-DNN modeled (a) Fe_{sol}% and (b) d-Fe concentrations in North Pacific aerosols, and for EA-XGBoost modeled (c) Fe_{sol}% and (d) d-Fe concentrations in the same samples.

https://doi.org/10.5194/egusphere-2026-1615
Preprint. Discussion started: 8 April 2026

3.5.2 Atlantic aerosols

The EA-DNN model successfully reproduced both Fe_{sol}% and d-Fe concentration in Atlantic aerosols as well as in North Pacific aerosols (Figure 7a and S10). The agreement between modeled and observed Fe_{sol}% over a broad range indicated that the model robustly captures the major variability in Fe_{sol}%. Such agreement suggests that Fe_{sol}% in Atlantic aerosols, as in North Pacific aerosols, can be described using relationships extracted from East Asian aerosol data. This further implies that the controls on Fe_{sol}% are not strictly region-specific, but instead reflect more general processes embedded in the model, including source characteristics, chemical processing during atmospheric transport, including aerosol acidification.

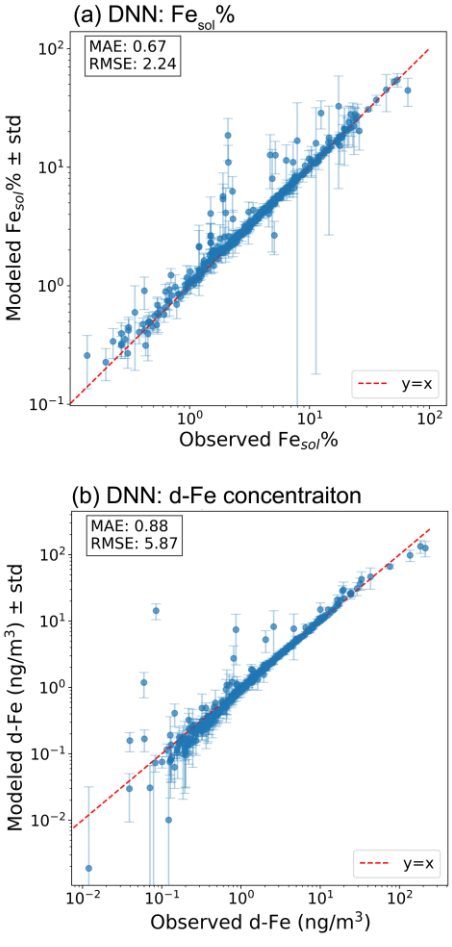

Figure 7. (a) The reproducing results of Fe_{sol}% in the Atlantic aerosols by EA-DNN model. (b) The same for d-Fe concentrations in the Atlantic aerosols.

A similar tendency is evident for d-Fe concentration (Figure 7b), where the modeled values also cluster around the 1:1 line. This agreement indicates that the model successfully reproduces dissolved Fe concentrations in North Pacific

https://doi.org/10.5194/egusphere-2026-1615
Preprint. Discussion started: 8 April 2026

aerosols. Because d-Fe concentration is controlled not only by Fe_{sol}% but also by total Fe abundance, particle composition, and transport and deposition processes, accurate reproduction requires the simultaneous representation of multiple interacting factors. The fact that a model trained exclusively on East Asian aerosols can also reproduce Atlantic aerosol samples therefore suggests that the EA-DNN model captures essential relationships governing aerosol Fe dissolution and dissolved Fe supply, rather than simply reflecting a local empirical relationship. Nevertheless, several samples depart from the 1:1 line, implying that additional factors not represented in the East Asian training dataset may have contributed to those cases. The reasons for these deviations are discussed in Section 3.7.

3.5.2 South Pacific aerosols

Finally, the EA-DNN model was applied to Fe_{sol}% and d-Fe concentration collected in the South Pacific Ocean. Although the South Pacific dataset is known to include samples significantly influenced by volcanic rock (Perron et al., 2021), the EA-DNN model successfully reproduced the Fe_{sol}% values (Figure 8a and S11). By contrast, the reproducibility of d-Fe concentrations decreased, most notably for samples with low d-Fe concentration (<1 ng m^{-3}, Figure 8b). Log–log plots primarily capture relative errors; thus, the relative absolute error (|observede d-Fe – modeled d-Fe|/observed d-Fe) increase substantially at low observed concentrations even when the absolute deviation is minor. In a linear–linear plot that highlights absolute errors (observation minus prediction), most samples exhibit acceptable reproducibility, excluding several outliers. To assess whether these outliers (i.e., samples with large relative error: RE = (observed Fe_{sol}% - modeled Fe_{sol}%)/modeled Fe_{sol}%) reflect any systematic bias related to aerosol composition, South Pacific aerosol samples were categorized into three groups: (G1) RE < 50%, (G2) RE > 50% with AE < 1 ng m^{-3}, and (G3) RE > 50% with AE > 1 ng m^{-3}. The key distinction of G1 from G2 and G3 is that RE is below 50% and that, for most samples, the modeled values lie close to the 1:1 line.

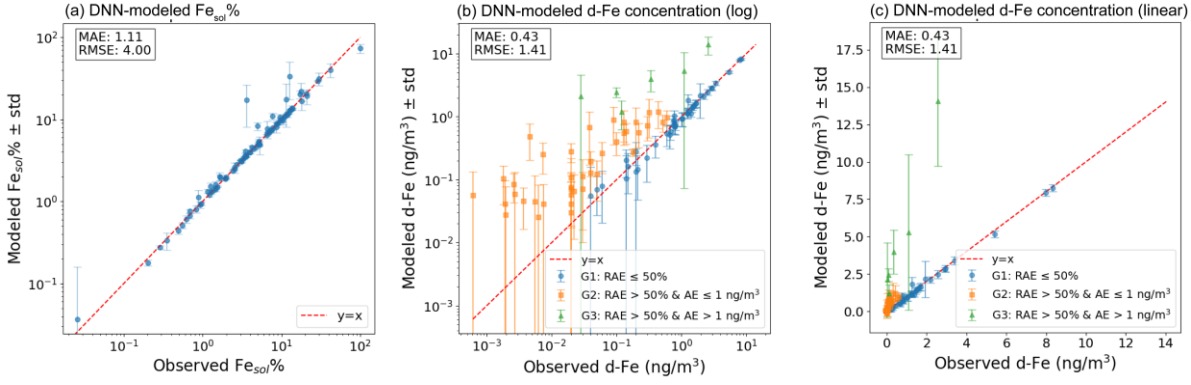

Figure 8. (a) DNN-modeled Fe_{sol}% and (b) DNN-modeled d-Fe concentrations in the South Pacific aerosols in log scale and (c) linear scale.

https://doi.org/10.5194/egusphere-2026-1615
Preprint. Discussion started: 8 April 2026

While [d-Fe]/[d-Al] and T-Fe/T-Al in G1 showed no significant difference from those in G2, the mean T-Fe concentration in G1 was approximately one order of magnitude higher than that in G2. As noted above, the East Asian dataset includes few samples with T-Fe concentrations as low as those in G2, suggesting that insufficient representation of low-T-Fe conditions in the training data contributed to the large RE in G2. In contrast, G3 exhibited markedly higher [d-Fe]/[d-Al] and T-Fe/T-Al than G1 and G2. These samples were collected in the coastal region of Australia and near the Big Ben volcano in Heard Island. Because volcanic rocks from the volcano are characterized by high T-Fe/T-Al, the elevated [d-Fe]/[d-Al] is plausibly attributable to volcanic inputs. In addition, aerosols in coastal Australia have been reported to be influenced by anthro-Fe, raising the possibility that the impact of anthro-Fe on Fe_{sol}% differs between the East Asian region and the Australian vicinity.

3.6 SHAP-ICA-based controlling factors across ocean basins

3.6.1 Fe_{sol}% in North Pacific aerosols

As shown in Figure 9a, the SHAP values for Alsol% and the [d-Fe]/[d-Al] ratio increased positively with increasing values of these variables, suggesting that chemical alterations of mineral dust and anthro-Fe is a key factor in enhancing Fe_{sol}%. By contrast, the SHAP values for T-Fe/T-Al become more negative as T-Fe/T-Al increases (Figure 9a). As discussed earlier, this pattern points to the emission of insoluble anthro-Fe and implied that simply emitting anthro-Fe into the atmosphere is insufficient to raise Fe_{sol}% of the North Pacific aerosols. The SHAP values for T-Fe concentration itself span only a narrow range, suggesting that T-Fe exerted a relatively minor influence on Fe_{sol}%.

Four ICs were extracted by applying ICA to these SHAP values. Among them, IC1 and IC2 contributed to variability in Fe_{sol}% in North Pacific aerosols (Figures 9b and 9c), whereas IC3 and IC4 were interpreted as residual components (Figures S12a and S12b). IC1 exhibited positive loadings on Al_{sol}% and [d-Fe]/[d-Al], whereas the contributions from T-Fe/T-Al and T-Fe were relatively small (Figure 10b). The IC1 scores were strongly correlated with the observed Fe_{sol}% (Figure 9b), indicating that Fe_{sol}% increased as atmospheric chemical alterations of mineral dust and anthro-Fe progressed. TSP samples with high IC1 scores were mainly distributed in the western and northern North Pacific (Figure 10d). Given that the subarctic North Pacific is an HNLC region, these results suggested that d-Fe was supplied in part by aerosols rendered soluble through chemical alterations in the atmosphere.

IC2 showed positive loadings for all four features, with T-Fe/T-Al and [d-Fe]/[d-Al] contributing most strongly, indicating that this component may be related to anthro-Fe (Figure 9c). Given that the chemical alteration of anthro-Fe was extracted as IC1, IC2 may represent direct emissions of anthro-Fe with high T-Fe/T-Al and [d-Fe]/[d-Al]. IC2 scores tended

https://doi.org/10.5194/egusphere-2026-1615
Preprint. Discussion started: 8 April 2026

to be higher along ~30°N and in the Gulf of Alaska (Figure 9e), which coincides with major shipping routes between East Asia and North America (Fujii et al., 2019; Hashimoto and Furusho, 2022). In particular, IC2 scores were high in the eastern Pacific far from East Asia (Figure 9e). Taking together, these features potentially point to fly ash from heavy-oil combustion as a plausible source. The weak positive correlation between IC2 scores and Fe_{sol}% suggests that these particles could have had relatively high Fe_{sol}% already at emission. However, the correlation between IC2 scores and Fe_{sol}% was weak, suggesting that the influence of IC2 on Fe_{sol}% in North Pacific aerosols is likely limited.

In summary, Fe_{sol}% in North Pacific aerosols were primarily regulated by atmospheric chemical alterations of mineral dust and anthro-Fe, while the HNLC region additionally shows signatures of fly ash from heavy-oil combustion that is highly soluble at emission. This implied that d-Fe in the subarctic North Pacific HNLC region was affected by both atmospheric processing and direct emissions of anthro-Fe with high Fe_{sol}% at the emissions. These findings demonstrated that extending SHAP analysis with ICA and visualizing IC scores in geographical space enables robust identification of the processes controlling Fe_{sol}%.

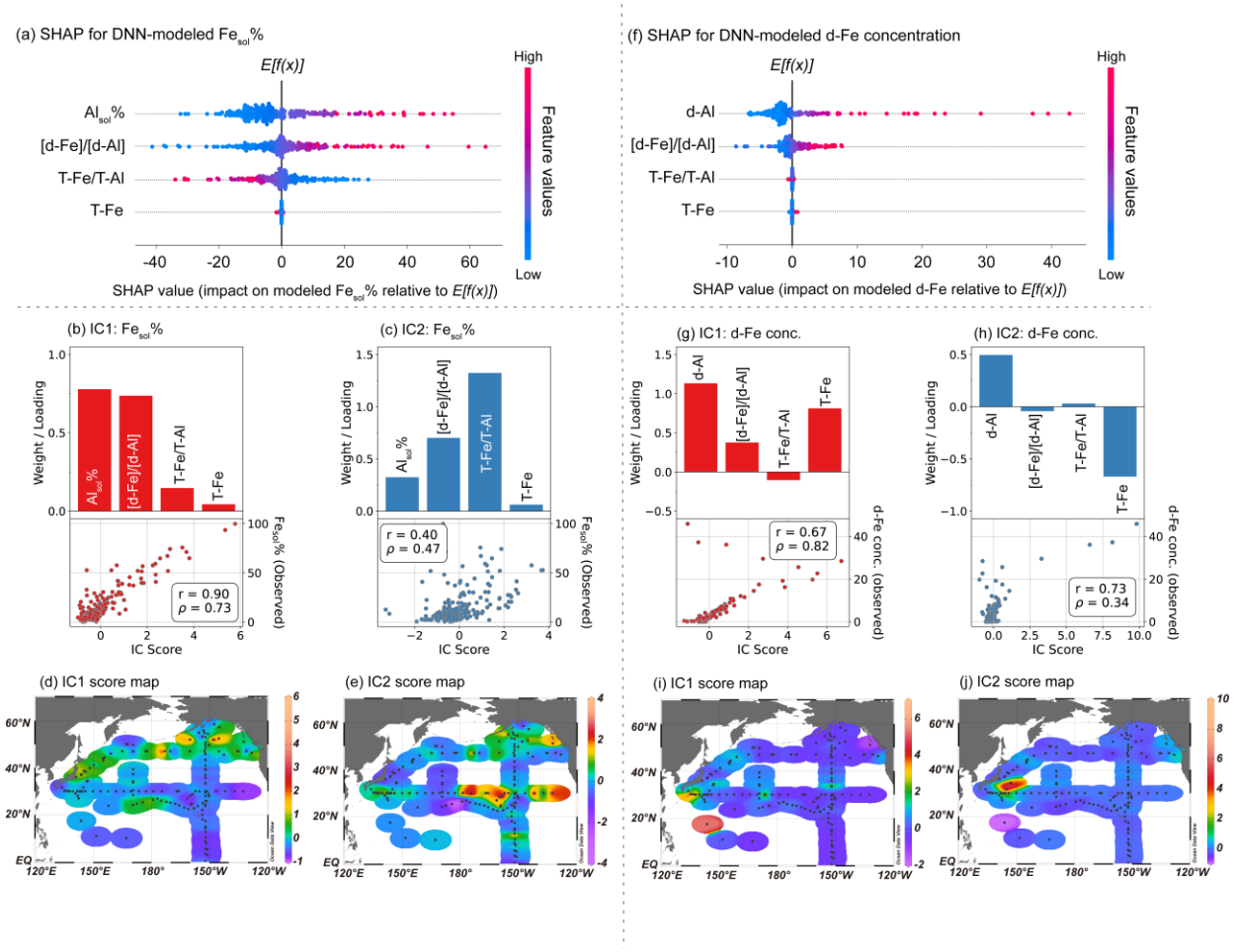

https://doi.org/10.5194/egusphere-2026-1615
Preprint. Discussion started: 8 April 2026

Figure 9. SHAP values DNN-modeled (a) Fe_{sol}% in the North Pacific aerosols. Characteristics of (b) IC1 and (c) IC2 and how they affect Fe_{sol}%. The upper bar plot indicates the feature loadings, and the lower scatter plot shows the relationship between IC score and observed Fe_{sol}%. Spatial distributions of scores of (d) IC1 and (e) IC2. (f-j) same for d-Fe concentration.

3.6.2 d-Fe concentration in North Pacific aerosols

For the DNN model reproducing d-Fe concentration, d-Al concentrations yielded the largest contribution, followed by the [d-Fe]/[d-Al] ratio (Figure 9f). By contrast, SHAP values for T-Fe/T-Al ratio and T-Fe concentration clustered near 0 (Figure 10f). This result indicated that d-Fe concentration in the North Pacific aerosols were mainly originated by Fe dissolution of mineral dust and anthro-Fe in the atmosphere, while the contributions of direct emission of d-Fe from anthropogenic emissions was minor.

Applying ICA to the SHAP values of the features for d-Fe concentration extracted two meaningful components and two residual components (Figures 9g, 9h, S10c, and S10d). These results indicate that d-Fe concentration is controlled by factors distinct from those governing Fe_{sol}%. In IC1, d-Al concentration and [d-Fe]/[d-Al], as well as T-Fe, showed positive loadings (Figure 8g). IC1 scores correlated well with the observed d-Fe concentrations, and the high IC1 scores were mainly found around the western North Pacific (Figure 9i). Taking together, these results suggested that d-Fe concentrations were largely determined by chemical alterations of mineral dust and anthro-Fe (d-Al concentration and [d-Fe]/[d-Al]), while the total transported loading of Fe-bearing aerosols, reflected by T-Fe, also constrained the magnitude of d-Fe supply to the North Pacific. This pattern was consistent with enhanced solubilization of mineral dust and anthro-Fe in East Asian urban outflow prior to long-range transport, followed by depositional loss that weakened the signal toward the remote ocean. In contrast, ICA for Fe_{sol}% showed stronger processing signals in the eastern North Pacific than in the western region. This likely arose because Fe_{sol}% was a fractional metric, defined as d-Fe relative to total Fe, such that strong processing yielded high values even over remote ocean regions where Fe transport was limited and d-Fe concentrations were low. Therefore, high Fe_{sol}% did not necessarily indicate a large d-Fe supply.

IC2 was characterized in the SHAP space by a strong positive contribution from d-Al concentration and a strong negative contribution from T-Fe concentration. The scatter plot between IC2 score and d-Fe concentration showed that North Pacific aerosols with high IC2 scores also exhibited high d-Fe concentrations, and these samples corresponded to outliers in the IC1 scatter plot (Figure 9h). These samples were mainly observed in the western Pacific and had T-Fe concentrations exceeding 1000 ng m^{-3} (Buck et al., 2006). Given that anthro-Fe contributed little to both T-Fe and d-Fe due to almost no contribution of T-Fe/T-Al and [d-Fe]/[d-Al] ratios (Figure 9h), these samples were interpreted as reflecting mineral dust–dominated dust events. During dust events, carbonate buffering (e.g., $CaCO_3$) can reduce aerosol acidity and thereby

https://doi.org/10.5194/egusphere-2026-1615
Preprint. Discussion started: 8 April 2026

relatively suppress acidification and dissolution of Fe-bearing particles. Thus, even under high dust loading with elevated T-Fe, the dissolution efficiency may decrease, and the model treated T-Fe as a downward adjustment term relative to the increase in d-Fe explained by d-Al, leading to the negative contribution of T-Fe in IC2. In contrast, IC1 showed a positive loading for T-Fe and d-Fe increased with increasing T-Fe. This likely reflected conditions under which acidification progressed in the East Asian atmosphere, particularly for fine particles, beyond carbonate buffering capacity, promoting Fe solubilization, such that an increased transported Fe loading to the North Pacific manifested as higher d-Fe concentrations.

3.6.3 Atlantic aerosols

The SHAP values for Fe_{sol}% in Atlantic aerosols were broadly consistent with those obtained for the Pacific. The analysis indicated that both the chemical alterations of mineral dust (Al_{sol}%) and the anthro-Fe ([d-Fe]/[d-Al]) contributed almost equally to the enhancement of Fe_{sol}% in the Atlantic (Figure 11a). For d-Fe concentration, d-Al was the most important feature, followed by [d-Fe]/[d-Al], implying that mineral dust was the dominant source of d-Fe in the Atlantic region (Figure 11f).

Applying ICA to the SHAP values extracted two dominant components (IC1 and IC2) that influence Fe_{sol}% and d-Fe concentrations (Figure 10), whereas the remaining two components mainly reflected residual or unexplained variation (Figure S13). IC1 scores, which reflected the chemical alterations of mineral dust and anthro-Fe, also correlated with observed Fe_{sol}%, but this correlation was weaker than that observed over the North Pacific (Figures9b and 10b). IC1 scores tended to be low near the Saharan outflow region, whereas they were higher in the European coastal region. This contrast suggested that Saharan dust did not undergo severe chemical alterations because it is transported without substantial influence from heavily polluted air masses, while aerosols near Europe are more strongly affected by anthropogenic acidic species, resulting in higher Fe_{sol}%. Moderately elevated IC1 scores were also observed in the western Atlantic. Previous studies have reported that aerosols over the Atlantic become internally mixed with sulfate and oxalate through cloud processing during transport (Fitzgerald et al., 2015). However, because the mean pH of Atlantic cloud water is around 5.0 (Shah et al., 2020), the scarcity of extremely solubilized samples likely reflects the limited acidity of cloud water.

In IC2, the largest positive loading was observed for T-Fe/T-Al, followed by [d-Fe]/[d-Al] and Alsol%, whereas T-Fe showed a slightly negative loading (Figure 10c). The loading structure of this component resembles that of the IC associated with heavy oil combustion from shipping identified in the North Pacific (Figure 8c). In the Atlantic dataset, elevated IC2 scores were mainly found in samples collected in the North Pacific. Importantly, the elevated IC2 scores in the subarctic North Pacific (>45°N) were consistently observed during two cruises: the CLIVAR/CO_2 Repeat Hydrography section A16N (a meridional transect along 20°W in June 2003; Buck et al., 2010a) and GA01 (a trans-basin North Atlantic cruise in June 2014; Chance et al., 2015). This finding likely reflected an aerosol emission source that was distinctive to the North Atlantic.

https://doi.org/10.5194/egusphere-2026-1615
Preprint. Discussion started: 8 April 2026

As in the North Pacific, IC1 showed the largest loading for d-Al, followed by T-Fe and then [d-Fe]/[d-Al], and the IC1 scores exhibited a clear linear relationship with d-Fe concentrations. The loading of [d-Fe]/[d-Al] was smaller than those of d-Fe and T-Fe, suggesting that chemical alteration of mineral dust is an important control on d-Fe concentrations in Atlantic aerosols, whereas the relative contribution of anthro-Fe is limited. Consistently, high IC1 scores were mainly observed in the coastal region adjacent to the Sahara Desert (Figure 10i). Considering that chemical alteration exerts a strong influence on Fe_{sol}% over the European offshore region and the western Pacific but a weaker influence near the Saharan coast, these results imply that the total transport of mineral dust underpins the supply of Fe to the Atlantic.

For IC2, d-Fe showed a positive loading while T-Fe showed a negative loading, and the anthro-Fe-related variables (T-Fe/T-Al and [d-Fe]/[d-Al]) contributed little. This indicates that IC2 primarily reflects processes associated with mineral dust. Most samples had IC2 scores clustered around zero, whereas a subset displayed high IC2 scores together with elevated d-Fe concentrations (Figure 10h). These samples correspond to outliers from the linear relationship between IC1 score and d-Fe were mainly located around ~30°W in the offshore Saharan Atlantic (Figures 10g and 10h). This pattern likely reflects a process in which Fe was deposited during transport from the Sahara toward ~30°W, while chemically altered mineral dust continued to be transported. Overall, while anthro-Fe may contribute to controlling Fe_{sol}% in the Atlantic, chemical alterations of mineral dust and its long-range transported were the dominant contributor from the perspective of d-Fe supply.

https://doi.org/10.5194/egusphere-2026-1615
Preprint. Discussion started: 8 April 2026

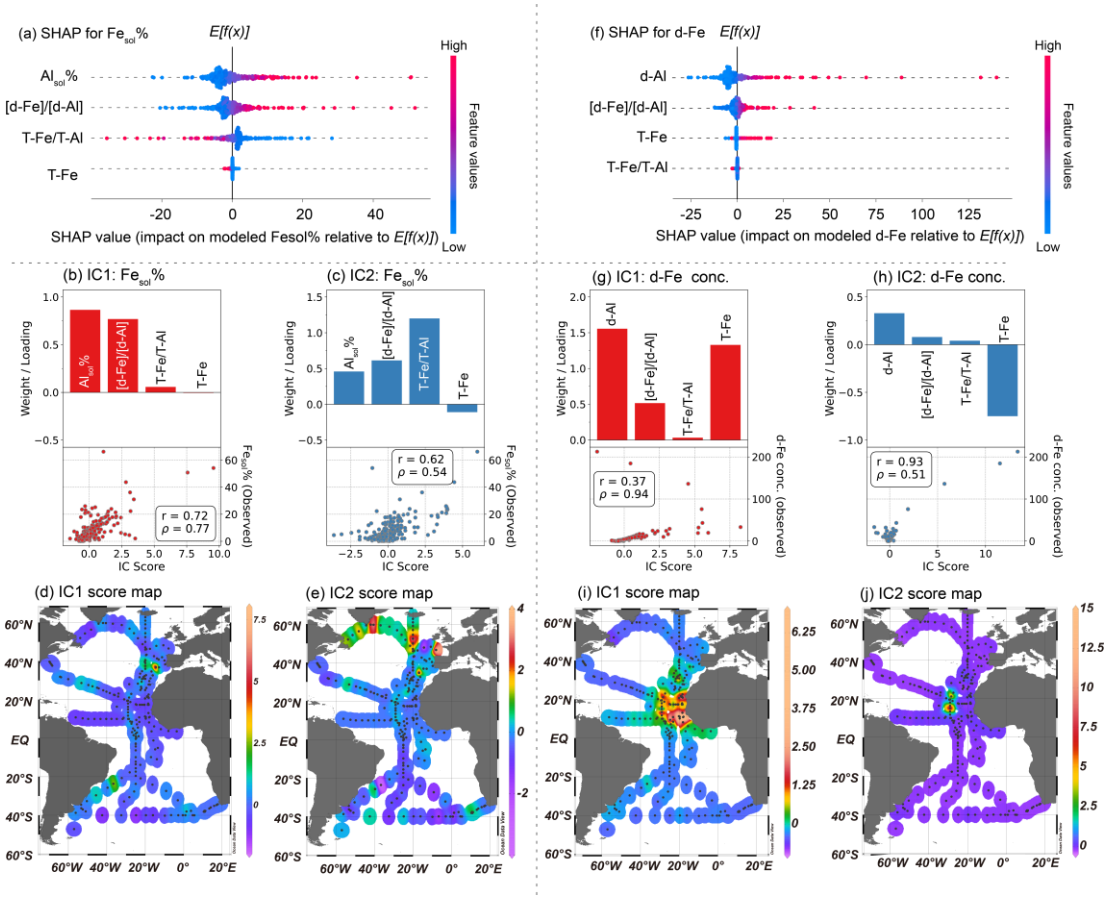

Figure 10. SHAP values DNN-modeled (a) Fe_{sol}% in the Atlantic aerosols. Characteristics of (b) IC1 and (c) IC2 and how they affect Fe_{sol}%. The upper bar plot indicates the feature loadings, and the lower scatter plot shows the relationship between IC score and observed Fe_{sol}%. Spatial distributions of scores of (d) IC1 and (e) IC2. (f-j) same for d-Fe concentration.

3.6.4 South Pacific aerosols

IC1 and IC2 were contributed to fluctuations of Fe_{sol}% and d-Fe concentrations in the South Pacific aerosols (Figure 11), whereas IC3 and IC4 mainly reflected residual or unexplained variation (Figure S14). SHAP values suggested that chemical processing of mineral dust and anthro-Fe (including volcanic rock with high T-Fe/T-Al, in the case of the South Pacific) positively contributed to Fe_{sol}% and d-Fe (Figures 11a and 11f). By contrast, T-Fe/T-Al and T-Fe either contributed negatively or exerted little influence (Figures 11a and 11f). Similar tendencies have been reported for other regions,

https://doi.org/10.5194/egusphere-2026-1615
Preprint. Discussion started: 8 April 2026

indicating that SHAP alone may not be sufficient to resolve regional differences in the factors controlling Fe_{sol}% and d-Fe concentration. In other words, the key processes governing Fe_{sol}% and d-Fe concentration are globally comparable and can be captured by training on the East Asian aerosol dataset.

For Fes_{ol}%, IC1 strongly reflected contributions from [d-Fe]/[d-Al] and Alsol% and showed a very strong correlation with observed Fe_{sol}% ($r = 0.96$, $\rho = 0.79$; Figure 11b). IC1 scores were generally higher in the region around Australia and the western sector, and lower along the central-to-eastern South Pacific transect (Figure 12d). These results suggested that Fe_{sol}% in South Pacific aerosols were primarily controlled by chemical alterations of mineral dust, with this influence most clearly expressed near the western source region.

By contrast, IC2 for Fe_{sol}% included contributions not only from [d-Fe]/[d-Al] and Alsol% but also from T-Fe/T-Al and T-Fe, and its correlation with observed Fe_{sol}% was weak ($r = 0.21$, $\rho = 0.54$; Figure 11c). The scatter plot between IC2 score and Fe_{sol}% shows no clear correlation. However, several samples with high IC2 scores coincided with relatively high Fe_{sol}%, suggesting that IC2 captures episodic influences that can elevate Fe_{sol}% under specific source regimes (Figure 11c). Spatially, IC2 scores were relatively high over the high-latitude southern Indian Ocean (~60–90°E, 40–60°S; Figure 11e), consistent with a potential contribution from volcanogenic particles from Heard Island, which may exhibit high T-Fe/T-Al and high [d-Fe]/[d-Al]. In addition, locally elevated IC2 scores were also found east of Australia (Figure 11e), where coastal influences could enhance the relative contribution of anthro-Fe. Nevertheless, given the overall weak relationship between IC2 and Fe_{sol}%, these volcanogenic and anthro-Fe influences appear to be local or episodic rather than a dominant control on basin-scale Fe_{sol}% variability.

For d-Fe concentrations, IC1 showed positive contributions from d-Al and [d-Fe]/[d-Al], as well as from T-Fe/T-Al (and T-Fe), and correlated strongly with observed d-Fe ($r = 0.91$, $\rho = 0.83$; Figure 11g). IC1 scores were higher around Australia and lower toward the central-to-eastern South Pacific (Figure 11i), suggesting that while d-Fe generation depends on chemical alterations, the absolute d-Fe concentrations are additionally influenced by the total transport and composition of mineral dust and anthro-Fe (T-Fe/T-Al and T-Fe), leading to higher concentrations near the western source region. In contrast, IC2 for d-Fe included contributions opposite to d-Al concentration and showed little correlation with observed d-Fe (Figure 12h), indicating that IC2 is not a primary driver of d-Fe variability in this dataset.

https://doi.org/10.5194/egusphere-2026-1615
Preprint. Discussion started: 8 April 2026

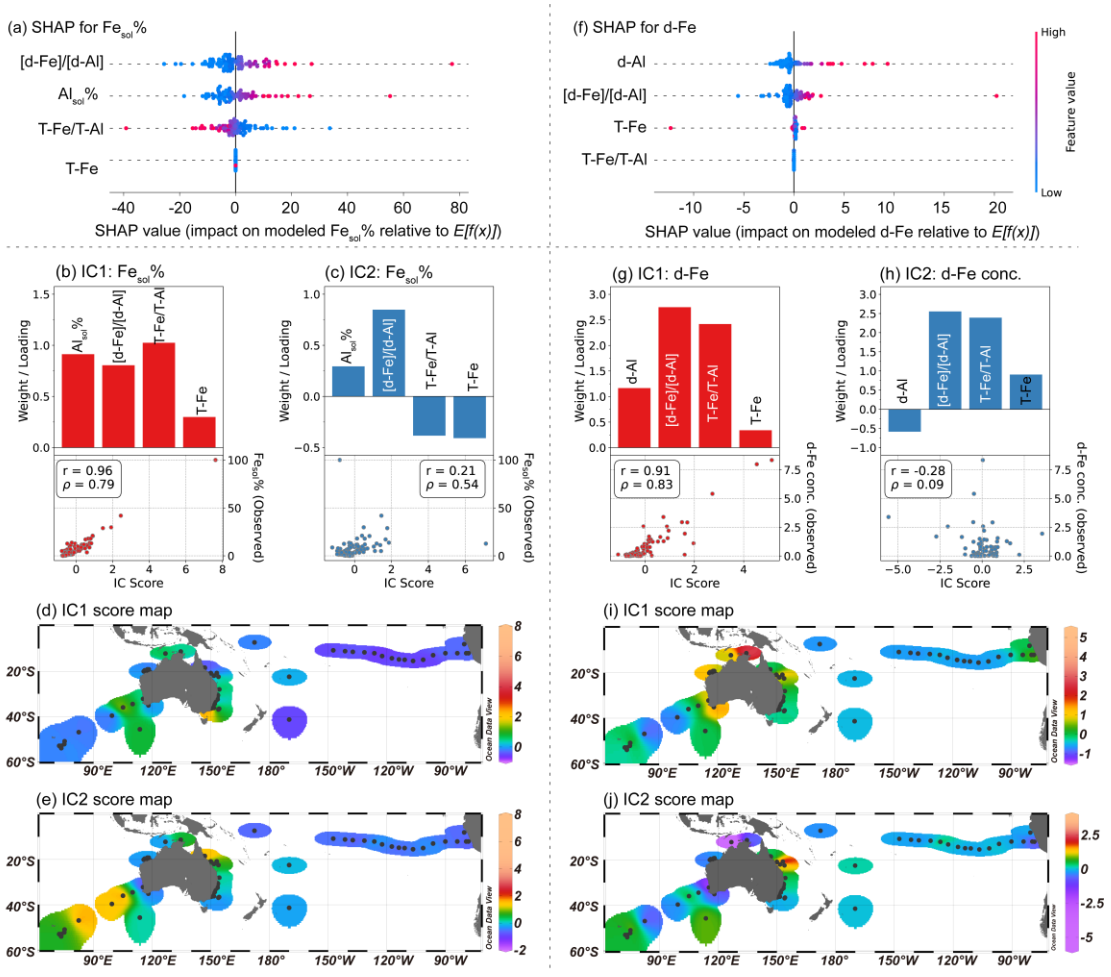

675 **Figure 11**. SHAP values DNN-modeled (a) Fe_{sol}% in the South Pacific aerosols. Characteristics of (b) IC1 and (c) IC2 and how they affect Fe_{sol}%. The upper bar plot indicates the feature loadings, and the lower scatter plot shows the relationship between IC score and observed Fe_{sol}%. Spatial distributions of scores of (d) IC1 and (e) IC2. (f-j) same for d-Fe concentration.

https://doi.org/10.5194/egusphere-2026-1615
Preprint. Discussion started: 8 April 2026

3.7 Characteristics of aerosol samples with low reproducibility

3.7.1 North Pacific aerosols

Out of 233 samples from the North Pacific Ocean, 23 were identified as low-reproducibility (absolute error (AE) > 3.0%), indicating that the EA-DNN model failed to adequately learn their characteristics. Analysing these samples is therefore crucial for identifying unlearned Fe emission sources or dissolution processes. These poorly reproduced samples were subsequently divided into two groups.

Group I comprises aerosol samples for which the modeled Fe_{sol}% exceeded the observed values. These samples are characterized by the following three features: (i) Al_{sol}% is higher than Fe_{sol}% (Figure 13a), (ii) the T-Fe/T-Al ratio is similar to or lower than that of mineral dust (T-Fe/T-Al: 0.52 ± 0.12, Figure 12b), and (iii) [d-Fe]/[d-Al] is less than 0.1 (Figure 12b). These characteristics align with aluminosilicate glass from coal combustion fly ash (Kukier et al., 2003; Sakata et al., 2023), but their appearance in only 10 samples implies that the contribution of this source to Fe over the North Pacific is likely minor. This result was supported by source apportionment of aerosol Fe using Fe isotope ratio (□56Fe). Previous studies have reported that the Fe isotopic ratio of coal fly ash ($\delta^{56}Fe$ = 0.05–0.80‰, Mead et al., 2013; Li et al., 2022) are higher than the average values for mineral dust ($\delta^{56}Fe$ = 0.10‰). Nevertheless, $\delta^{56}Fe$ higher than 0.10‰ has rarely observed in fine aerosol particles collected in the North Pacific aerosols (Kurisu et al., 2021, 2024).

Although aluminosilicate glasses from coal combustions exhibited minor contribution to Fe_{sol}% regulation in the North Pacific aerosols, previous studies have reported that coal combustion is a major emission source of anthro-Fe in North Pacific aerosols (Kurisu et al., 2021, 2024). This finding appears to contradict our result that the contribution of coal combustion derived aluminosilicate glass was small. However, this discrepancy can be explained by the existence of two types of anthro-Fe derived from coal combustion with different formation processes. These include aluminosilicate glass, formed by the melting of clay minerals and SiO_2 in the furnace followed by rapid quenching, and Fe-oxide nanoparticles, which aggregate from vaporized Fe. Notably, the low isotope ratios ($\delta^{56}Fe$ < 0‰) of the iron oxide nanoparticles, caused by kinetic isotope effects during Fe vaporization, correlated with the EF of Pb, a tracer for coal combustion. Furthermore, greater contribution of anthro-Fe leads to higher Fe_{sol}% and [d-Fe]/[d-Al] ratios in North Pacific aerosols (Sakata et al., 2023; Kurisu et al., 2024), consistent with the SHAP analysis, which shows that larger SHAP values for [d-Fe]/[d-Al] correspond to higher Fe_{sol}% (Figure 9a). Thus, the EA-DNN model developed in this study successfully distinguishes different anthro-Fe species, such as Fe oxide nanoparticles and aluminosilicate glass, and quantifies their respective contributions to Fe_{sol}%.

Group II consisted of aerosol samples for which the EA-DNN underestimated Fe_{sol}% relative to the observations (Figure 13a). These samples generally had Fe_{sol}% exceeding Alsol% and showed a weak positive correlation between [d-Fe]/[d-Al] and T-Fe/T-Al (Figure 12c). Given that the EA-DNN accurately reproduced high Fe_{sol}% associated with

https://doi.org/10.5194/egusphere-2026-1615
Preprint. Discussion started: 8 April 2026

atmospheric processing, the remaining underestimation most likely reflected insufficient training data for anthro-Fe with high Fe_{sol}% at emission. Heavy oil combustion is a plausible candidate because its Fe_{sol}% value is above 38% (Schroth et al., 2009; Oakes et al., 2012). This interpretation is consistent with the importance of heavy oil combustion along the major North Pacific shipping route between East Asia and North America (Ito, 2013; Fujii et al., 2019; Hashimoto and Furusho, 2022) and with previous reports that T-Fe/T-Al and [d-Fe]/[d-Al] increase with heavy oil contributions (Figure 10c, Sedwick et al., 2007; Sakata et al., 2023). This interpretation was further supported by the fact that the spatial distribution of samples showing large differences between observed and modeled Fe_{sol}% resembled that of IC2 score (Figure 9c), which reflected the influence of heavy oil combustion. Thus, the outlier analysis also demonstrated that potential emission sources can be inferred from the characteristic features of underrepresented samples in the training data.

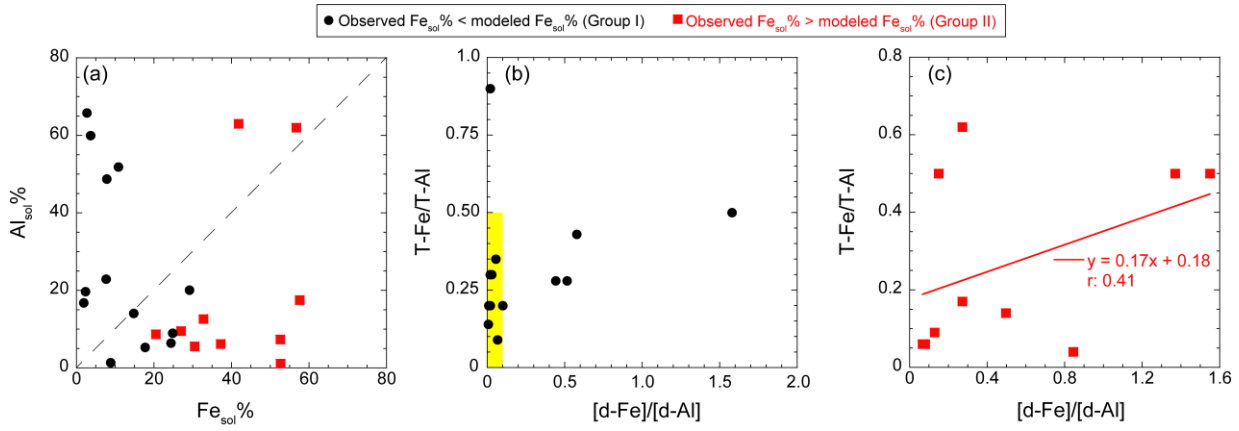

Figure 12. (a) A scatter plot between observed Fe_{sol}% and Al_{sol}% in the North Pacific aerosol particles with AE > 3.0%. The diagram of T-Fe/T-Al versus [d-Fe]/[d-Al] for North Pacific aerosols with low reproducibility, showing: (b) samples where Fe_{sol}% was overestimated, and (c) samples where Fe_{sol}% was underestimated by the DNN model.

3.7.2 Atlantic aerosols

Nineteen Atlantic aerosol samples with low reproducibility (absolute errors greater than 3.0%) were categorized into two groups. Group I included 18 samples where the model underestimated Fe_{sol}%. Samples in Group I are characterized by higher Al_{sol}% than Fe_{sol}% and by [d-Fe]/[d-Al] ratios below 0.1 (Figures 13a and 13b). This feature is consistent with that of the North Pacific aerosols in Group I aerosols over the North Pacific, which exhibit low reproducibility (Figures 12a and 12b). These features were similar to aluminosilicate glass originating from high-temperature combustion. These characteristics also aligned with aluminosilicate glass derived from high-temperature combustion, and the low reproducibility was likely due to insufficient training on aerosol samples strongly influenced by aluminosilicate glass.

https://doi.org/10.5194/egusphere-2026-1615
Preprint. Discussion started: 8 April 2026

In contrast, for the remaining sample, the model underestimated Fe_{sol}%. In this case, the observed Fe_{sol}% was lower than Al_{sol}%, resembling the characteristics of Group II aerosols over the North Pacific, which also show low reproducibility (Figures 12a and 12b). In the North Pacific, such characteristics are considered to reflect contributions from heavy oil combustion. However, in the Atlantic, since only one corresponding sample is available, a clear attribution is difficult. Nevertheless, the influence on Fe_{sol}% in Atlantic aerosols is likely to be minor.

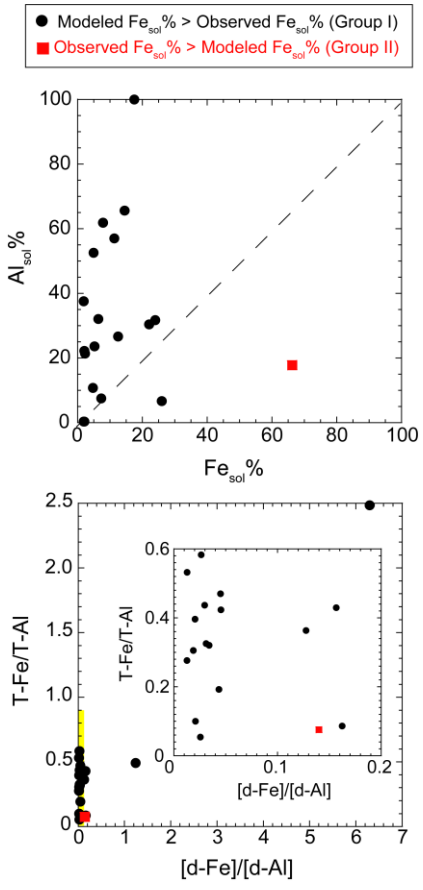

Figure 13. (a) A scatter plot between observed Fe_{sol}% and Al_{sol}% in the Atlantic aerosols with AE > 3.0%. (b) The diagram of T-Fe/T-Al versus [d-Fe]/[d-Al] for the Atlantic aerosols with low reproducibility.

https://doi.org/10.5194/egusphere-2026-1615
Preprint. Discussion started: 8 April 2026

4. Implications

4.1 Global commonality of processes controlling aerosols Fe_{sol}% and d-Fe concentrations

Although aerosols over the Atlantic and South Pacific are expected to almost no direct influence from East Asian outflow, both Fe_{sol}% and d-Fe concentrations in aerosol particles collected in these regions were well reproduced by the EA-DNN model. This agreement suggested that similar underlying processes control Fe_{sol}% and d-Fe concentrations on a global scale. This is likely because both the chemical species of mineral dust and anthro-Fe at emission (which govern the initial values of Fe_{sol}%) and the elementary reaction pathways during their subsequent alteration (which drive increases in Fe_{sol}%) can fundamentally be described by similar functional relationships. For instance, although Asian dust and Saharan dust differ in their bulk mineral compositions, their Fe-bearing mineral phases have been reported to be similar and to consist mainly of illite–smectite clays, biotite, chlorite, kaolinite, and Fe-oxide inclusions (Guodie and Middleton, 2001; Takahashi et al., 2011; Jeong and Achterberg, 2014; Jeong and Nousiainen, 2014; Jeong, 2016, 2024; Rodriguez-Navarro et al., 2018). Moreover, in the case of anthro-Fe, contributions from steel industry and NEV particles are reported to be large worldwide, indicating that the Fe species emitted from these sources (predominantly Fe-oxides) are also likely to be comparable on a global scale.

The second reason is that the elementary reaction processes of Fe-bearing particles are likely to be similar on a global scale. In East Asia, Fe in fine aerosol particles was predominantly solubilized, and these particles underwent chemical alterations by sulfate and oxalate. As evidence for this, many Fe-bearing particles in the fine fraction were internally mixed with sulfate and oxalate, resulting in the formation of iron sulfate and iron oxalate. Particles internally mixed with acidic anions and oxalate derived from such species have also been observed in aerosols collected over the North Pacific and the Atlantic. This suggests that the acidic species and organic acids responsible for Fe solubilization are fundamentally similar across regions, and that differences in solubility are likely governed primarily by the pH during reaction. In fact, Fe-bearing particles in East Asia are thought to be altered mainly through heterogeneous reactions with SO_2 under highly acidic conditions ($pH < 3$) before being transported over the Pacific, whereas Atlantic aerosols are considered to undergo weathering and alteration primarily through in-cloud processes under moderately acidic conditions (Fitzgerald et al., 2015; Dall'Osto et al., 2010; Kandler et al., 2011; Denjean et al., 2015; Zhah et al., 2020).

Although aerosol Fe dissolution likely occurred under different conditions (e.g., aerosol acidity) in the North Pacific and the North Atlantic, the EA-DNN was able to reproduce the variability in Fe_{sol}% reasonably well. This is probably because the East Asian training dataset broadly includes aerosols spanning Fe_{sol}% from extremely low values (approximately 0.01%) to nearly 100%. On the other hand, the alteration of mineral particles and anthro-Fe is likely influenced by multiple processes, including proton-promoted and ligand-promoted dissolutions. Using the [d-Fe]/[d-Al] versus enrichment factor of Fe (or T-Fe/T-Al ratio) diagram employed in Part I, it is possible to qualitatively assess which process contributed more to

https://doi.org/10.5194/egusphere-2026-1615
Preprint. Discussion started: 8 April 2026

Fe dissolution from mineral dust, whereas such qualitative evaluation is difficult for anthro-Fe. Therefore, the effects of these mechanisms on Fe_{sol}% cannot yet be evaluated quantitatively. From a mechanistic perspective, features such as Alsol% and [d-Fe]/[d-Al] should also vary with aerosol pH and with the mixing state with sulfate, oxalate, and other related species. Accordingly, as attempted by Shi et al. (2022), the model should be further developed within a framework that explicitly includes the concentrations of sulfate, oxalate, and other relevant species, and analyses are also required to clarify the drivers of variability in Alsol% and [d-Fe]/[d-Al]. To achieve this, constructing more comprehensive observational databases that include these species is indispensable.

4.2 Revisiting the reason for the inverse relationship between T-Fe concentration and Fe_{sol}%

Previous studies reported an inverse relationship between Fe_{sol}% and T-Fe concentration (Sholkovitz et al., 2012; Mahowald et al., 2018). This has been explained by two mechanisms: (i) preferential deposition of mineral dust with low Fe_{sol}% in coarse aerosol particles, which leaves fine aerosol particles enriched in anthro-Fe with high Fe_{sol}%, and (ii) chemical alteration of Fe during atmospheric transport, which increases Fe_{sol}% as aerosols age and interact with pollutants. In both cases, T-Fe concentration decreases while Fe_{sol}% increases as transport time increases. Thus, the observed inverse relationship by itself does not allow us to identify which mechanism is dominant.

In Part I, inverse relationships between concentration and Fe_{sol}% for both mineral dust and anthro-Fe were found, suggesting that the chemical alterations of these aerosols were likely more important for the overall inverse correlation. These findings were further supported by reproducing Fe_{sol}% by XGBoost and DNN models. In particular, the IC scores related to the chemical alterations of mineral dust and anthro-Fe, as derived from SHAP-ICA, showed strong correlations with the observed Fe_{sol}%, whereas the IC scores representing the emission processes of these particles did not. This result highlighted that variations in aerosol Fe_{sol}% cannot be explained solely by changes in the mixing ratio of mineral dust and anthropogenic Fe (i.e., physical processes such as particle emission and deposition), and that chemical alteration processes are indispensable.

5. Conclusions

In this study, a predictive model for reproducing aerosol Fe_{sol}% and dissolved Fe (d-Fe) concentrations was constructed using an East Asian aerosol dataset and then applied to marine aerosols. XGBoost reproduced Fe_{sol}% and d-Fe concentrations well for aerosols within East Asia, but its performance deteriorated for marine aerosols. In contrast, the deep neural network (DNN) successfully captured the variability of Fe_{sol}% and d-Fe concentrations even in marine aerosols. This

https://doi.org/10.5194/egusphere-2026-1615
Preprint. Discussion started: 8 April 2026

is likely because the DNN can more appropriately represent the nonlinear relationships between the target variables and the input features, resulting in a model with higher generalization performance.

Interpretation of the model using SHAP analysis demonstrated that chemical alteration of aerosols plays a key role in controlling the variability of Fe_{sol}% and d-Fe concentrations. However, SHAP results alone showed only limited regional differences, making it difficult to explicitly compare how the controlling factors vary among regions. To address this, ICA was applied to the SHAP values for each sample, decomposing the co-variation of SHAP values among features into statistically independent components. As a result, particularly for d-Fe concentrations, the dominant controlling factors were found to differ between regions. For example, IC1 for d-Fe was highest over the western North Pacific, indicating a stronger influence of chemically processed Fe transported from East Asia, whereas the processing signal for Fe_{sol}% was more pronounced in the eastern North Pacific. Thus, combining the DNN model with SHAP and ICA for analysing the drivers of variability in Fe_{sol}% and d-Fe concentrations was shown to be highly useful for elucidating the controlling factors of these parameters.

In this study, the alteration of mineral dust and anthro-Fe was captured using Alsol% and [d-Fe]/[d-Al]. Ideally, these proxies could be parameterized directly by aerosol acidity, represented by sulfate and nitrate concentrations, together with oxalate concentration. Because the available datasets for these chemical indicators were limited, we could not explicitly incorporate them into the model. Expanding datasets for sulfate, nitrate, and oxalate and constructing DNN models for Fe_{sol}% and d-Fe using these variables are expected to provide a more detailed understanding of aerosol-mediated Fe supply processes to the ocean surface.

https://doi.org/10.5194/egusphere-2026-1615
Preprint. Discussion started: 8 April 2026

Code and data availability

Data archiving is underway in Zenodo, and the dataset will be made publicly available via Zenodo upon acceptance (doi: 10.5281/zenodo.19186414).

Supplement link

The link to the supplement will be included by Copernicus, if applicable.

Author contributions

KS and YT designed this study. KS and MT compiled dataset using this study. KS developed the model code and performed the simulations. KS prepared the manuscript with contributions from all co-authors.

Competing interests

The authors declare no conflicts of interest relevant to this study.

Disclaimer

Copernicus Publications adds a standard disclaimer: "Copernicus Publications remains neutral with regard to jurisdictional claims made in the text, published maps, institutional affiliations, or any other geographical representation in this paper. While Copernicus Publications makes every effort to include appropriate place names, the final responsibility lies with the authors. Views expressed in the text are those of the authors and do not necessarily reflect the views of the publisher."
Please feel free to add disclaimer text at your choice, if applicable.

Acknowledgements

The International GEOTRACES program is possible in part thanks to the support from the U.S. National Science Foundation (Grant OCE-2140395) to the Scientific Committee on Oceanic Research (SCOR). This paper also contributes to the science plan of the Surface Ocean-Lower Atmosphere Study (SOLAS), which is partially supported by the U.S. National Science Foundation (Grant OCE-1840868) via the Scientific Committee on Oceanic Research (SCOR).

https://doi.org/10.5194/egusphere-2026-1615
Preprint. Discussion started: 8 April 2026

Review statement

The review statement will be added by Copernicus Publications listing the handling editor as well as all contributing referees according to their status anonymous or identified.

References

Alexander, B., Park, R. J., and Jacob, D. J.: Transition metal-catalyzed oxidation of atmospheric sulfur: Global implications for the sulfur budget, J. Geophys. Res., 114, D02309, https://doi.org/10.1029/2008JD010486, 2009.

Alin, A: Multicollinearity, WIREs Comput. Stat., 2, 370–374, https://doi.org/10.1002/wics.84, 2010.

Baker, A. R., Jickells, T. D., Witt, M., and Linge, K.: Trends in the solubility of iron, aluminium, manganese and phosphorus in aerosol collected over the Atlantic Ocean, Mar. Chem., 98, 43–58, https://doi.org/10.1016/j.marchem.2005.06.004, 2006.

Buck, C. S., Landing, W. M., Resing, J. A., and Lebon, G.: Aerosol iron and aluminum solubility in the northwest Pacific Ocean: Results from the 2002 IOC cruise, Geochem. Geophys. Geosyst., 7, Q04M07, https://doi.org/10.1029/2005GC000977, 2006.

Buck, C. S., Landing, W. M., Resing, J. A., and Measures, C.: The solubility and deposition of aerosol Fe and other trace elements in the North Atlantic Ocean: Observations from the A16N CLIVAR/CO2 repeat hydrography section, Mar. Chem., 120, 57–70, https://doi.org/10.1016/j.marchem.2008.08.003, 2010.

Buck, C. S., Landing, W. M., and Resing, J.: Pacific Ocean aerosols: Deposition and solubility of iron, aluminum, and other trace elements, Mar. Chem., 157, 117–130, https://doi.org/10.1016/j.marchem.2013.09.005, 2013.

Chan, J. Y. L., Leow, S. M. H., Bea, K. T., Cheng, W. K., Phoong, S. W., Hong, Z. W., and Chen, Y.: Mitigating the multicollinearity problem and its machine learning approach: A review, Mathematics, 10, 1283, https://doi.org/10.3390/math10081283, 2022.

Chance, R., Jickells, T. D., and Baker, A.: Atmospheric trace metal concentrations, solubility and deposition fluxes in remote marine air over the south-east Atlantic, Mar. Chem., 177, 45–56, https://doi.org/10.1016/j.marchem.2015.06.028, 2015.

Chen, T., Guestrin, C: XGBoost: A scalable tree boosting system, Proc. 22nd ACM SIGKDD Int. Conf. Knowl. Discov. Data Min., 785–794. ACM, https://doi.org/10.1145/2939672.2939785, 2016.

Conway, T. M., Hamilton, D. S., Shelley, R. U., Aguilar-Islas, A. M., Landing, W. M., Mahowald, N. M., and John, S. G.: Tracing and constraining anthropogenic aerosol iron fluxes to the North Atlantic Ocean using iron isotopes, Nat. Commun., 10, 2628, https://doi.org/10.1038/s41467-019-10457-w, 2019.

Cui, W., Song, X., Su, Y., Chen, X., and Wu, D.: Soluble iron in source-based anthropogenic PM2.5 predominantly from steel industry and residential combustion in China, Geophys. Res. Lett., 52, e2025GL118603, https://doi.org/10.1029/2025GL118603, 2025.

Dall'Osto, M., Harrison, R. M., Highwood, E. J., O'Dowd, C., Ceburnis, D., Querol, X., and Achterberg, E.: Variation of the mixing state of Saharan dust particles with atmospheric transport, Atmos. Environ., 44, 3135–3146, https://doi.org/10.1016/j.atmosenv.2010.05.030, 2010.

Denjean, C., Caquineau, S., Desboeufs, K., Maille, L. M., Quinones Rosado, M., and Vallejo, P.: Long-range transport across the Atlantic in summertime does not enhance the hygroscopicity of African mineral dust, Geophys. Res. Lett., 42, 7835–7843, https://doi.org/10.1002/2015GL065693, 2015.

Fang, T., Guo, H., Zeng, L., Verma, V., Nenes, A., and Weber, R.: Highly acidic ambient particles, soluble metals, and oxidative potential: A link between sulfate and aerosol toxicity, Environ. Sci. Technol., 51, 2611–2620, https://doi.org/10.1021/acs.est.6b06151, 2017.

https://doi.org/10.5194/egusphere-2026-1615
Preprint. Discussion started: 8 April 2026

Fitzgerald, E., Ault, A. P., Zauscher, M. D., Mayol-Bracero, O. L., and Prather, K.: Comparison of the mixing state of long-range transported Asian and African mineral dust, Atmos. Environ., 115, 19–25, https://doi.org/10.1016/j.atmosenv.2015.04.031, 2015.

Fujii, M., Hashimoto, H., Taniguchi, Y., Kobayashi, E: Statistical validation of a voyage simulation model for ocean-going ships using satellite AIS data, J. Mar. Sci. Technol., 24, 1297–1307, https://doi.org/10.1007/s00773-019-00626-3, 2019.

Goudie, A. S., and Middleton, N.: Saharan dust storms: nature and consequences, Earth-Sci. Rev., 56, 179–204, https://doi.org/10.1016/S0012-8252(01)00067-8, 2001.

Gui, K., Che, H., Zeng, Z., Wang, Y., Zhai, S., and Wang, Z.: Construction of a virtual PM2.5 observation network in China based on high-density surface meteorological observations using the Extreme Gradient Boosting model, Environ. Int., 141, 105801, https://doi.org/10.1016/j.envint.2020.105801, 2020.

Halle, L. L., Palmqvist, A., Kampmann, K., Jensen, A., Hansen, T., and Khan, F.: Tire wear particle and leachate exposures from a pristine and road-worn tire to Hyalella azteca: Comparison of chemical content and biological effects, Aquat. Toxicol., 232, 105769, https://doi.org/10.1016/j.aquatox.2021.105769, 2021.

Hamilton, D. S., Perron, M. M. G., Bond, T. C., Bowie, A. R., Buchholz, R. R., and Guieu, C.: Earth, wind, fire, and pollution: Aerosols nutrient sources and impacts on ocean biogeochemistry, Annu. Rev. Mar. Sci., 14, 303–330, https://doi.org/10.1146/annurev-marine-031921-013612, 2022.

Harris, E., Sinha, B., van Pinxteren, D., Tilgner, A., Fomba, K. W., and Schneider, J.: Enhanced role of transition metal ion catalysis during in-cloud oxidation of SO2, Science, 340, 727–730, https://doi.org/10.1126/science.123091, 2013.

Hashimoto, H., Furusho, K: Influence of sea areas and season in navigation on the ship vulnerability to the parametric rolling failure mode, Ocean Eng., 266, 112714, https://doi.org/10.1016/j.oceaneng.2022.112714, 2022.

Hsieh, C. C., Chen, H. Y., and Ho, T. Y.: The effect of aerosol size on Fe solubility and deposition flux: A case study in the East China Sea, Mar. Chem., 241, 104106, https://doi.org/10.1016/j.marchem.2022.104106, 2022.

Hsieh, C. C., and Ho, T.: Contribution of anthropogenic and lithogenic aerosol Fe in the East China Sea, J. Geophys. Res.-Oceans, 129, e2024JC021113, https://doi.org/10.1029/2024JC021113, 2024.

Hsieh, C. C., You, C. F., and Ho, T.: The solubility and deposition flux of East Asian aerosol metals in the East China Sea: The effects of aeolian transport processes, Mar. Chem., 253, 104268, https://doi.org/10.1016/j.marchem.2023.104268, 2023.

Ito, A: Global modeling study of potentially bioavailable iron input from shipboard aerosol sources to the ocean, Global Biogeochem. Cy., 27, 1–10, https://doi.org/10.1029/2012GB004378, 2013.

Ito, A., Miyakawa, T: Aerosol iron from metal production as a secondary source of bioaccessible iron, Environ. Sci. Technol., 57, 4091–4100, https://doi.org/10.1021/acs.est.2c06472, 2023.

Ito, A., Shi, Z: Delivery of anthropogenic bioavailable iron from mineral dust and combustion aerosols to the ocean, Atmos. Chem. Phys., 16, 85–99, https://doi.org/10.5194/acp-16-85-2016, 2016.

Ito, A., Ye, Y., Baldo, C., Shi, Z: Ocean fertilization by pyrogenic aerosols iron, npj Clim. Atmos. Sci., 4, 30, https://doi.org/10.1038/s41612-021-00185-8, 2021.

Jeong, G. Y: Mineralogical properties and internal structures of individual fine particles of Saharan dust, Atmos. Chem. Phys., 16, 12397–12410, https://doi.org/10.5194/acp-16-12397-2016, 2016.

Jeong, G. Y: Microanalysis and mineralogy of Asian and Saharan dust, J. Anal. Sci. Technol., 15, 10, https://doi.org/10.1186/s40543-024-00425-5, 2024.

Jeong, G. Y., and Achterberg, E.: Chemistry and mineralogy of clay minerals in Asian and Saharan dusts and the implications for iron supply to the oceans, Atmos. Chem. Phys., 14, 12415–12428, https://doi.org/10.5194/acp-14-12415-2014, 2014.

Jeong, G. Y., Nouisiainen, T: TEM analysis of the internal structures and mineralogy of Asian dust particles and the implications for optical modeling, Atmos. Chem. Phys., 14, 7233–7254, https://doi.org/10.5194/acp-14-7233-2014, 2014.

https://doi.org/10.5194/egusphere-2026-1615
Preprint. Discussion started: 8 April 2026

Jickells, T. D., An, Z. S., Andersen, K. K., Baker, A. R., Bergametti, G., and Brooks, N.: Global iron connections between desert dust, ocean biogeochemistry, and climate, Science, 308, 67–71, https://doi.org/10.1126/science.1105959, 2005.

Kajino, M., Hagino, H., Fujitani, Y., Morikawa, T., Fukui, T., Onishi, K., Okuda, T., and Kajikawa, T.: Modeling transition metals in East Asia and Japan and its emission sources, GeoHealth, 4, e2020GH000259, https://doi.org/10.1029/2020GH000259, 2020.

Kandler, K., Schütz, L., Jäckel, S., Lieke, K., Emmel, C., and Müller-Ebert, D.: Ground-based off-line aerosol measurements at Praia, Cape Verde, during the Saharan Mineral Dust Experiment: microphysical properties and mineralogy, Tellus B, 63, 459–474, https://doi.org/10.1111/j.1600-0889.2011.00546.x, 2011.

König, D., Conaway, T. M., Hamilton, D. S., Tagliabue, A: Surface ocean biogeochemistry regulates the impact of anthropogenic aerosols Fe deposition on the cycling of iron and iron isotopes in the North Pacific, Geophys. Res. Lett., 49, e2022GL098016, https://doi.org/10.1029/2022GL098016, 2022.

Kukier, U., Ishak, C. F., Sumner, M. E., and Miller, W. P.: Composition and element solubility of magnetic and non-magnetic fly ash fractions, Environ. Pollut., 123, 255–266, https://doi.org/10.1016/S0269-7491(02)00376-7, 2003.

Kurisu, M., Adachi, K., Sakata, K., Takahashi, Y: Stable isotope ratios of combustion iron produced by evaporation in a steel plant, ACS Earth Space Chem., 3, 588–598, https://doi.org/10.1021/acsearthspacechem.8b00171, 2019.

Kurisu, M., Sakata, K., Nishioka, J., Obata, H., Conway, T. M., and Hunt, H. R.: Source and fate of atmospheric iron supplied to the subarctic north pacific traced by stable iron isotope ratios, Geochim. Cosmochim. Ac., 378, 168–185, https://doi.org/10.1016/j.gca.2024.06.009, 2024.

Kurisu, M., Sakata, K., Uematsu, M., Ito, A., Takahashi, Y: Contribution of combustion Fe in marine aerosols over the northwestern Pacific estimated by Fe stable isotope ratio, Atmos. Chem. Phys., 21, 16027–16050, https://doi.org/10.5194/acp-21-16027-2021, 2021.

Kurisu, M., Takahashi, Y: Testing iron stable isotope ratios as signature of biomass burning, Atmosphere, 10, 76, https://doi.org/10.3390/atmos10020076, 2019.

Kurisu, M., Takahashi, Y., Iizuka, T., Uematsu, M: Very low isotope ratio of iron in fine aerosols related to its contribution to the surface ocean, J. Geophys. Res. Atmos., 121, 11119–11136, https://doi.org/10.1002/2016JD024957, 2016.

Kurisu, M., Zhu, C., Miyakawa, T., Ito, A., Suzuki, K., Kashiwabara, T: Identification of anthropogenic Fe originated from East Asia using Fe stable isotope ratios of aerosols collected on Fukue Island, Atmos. Environ., 121893, https://doi.org/10.1016/j.atmosenv.2026.121893, 2026.

Li, J., An, X., Li, Q., Wang, C., Yu, H., Zhou, X., and Geng, Y.: Application of XGBoost algorithm in the optimization of pollutant concentration, Atmos. Res., 276, 106238, https://doi.org/10.1016/j.atmosres.2022.106238, 2022.

Li, R., Zhang, H., Wang, F., He, Y., Huang, C., Luo, L., Dong, S., and Jia, X.: Mass fractions, solubility, speciation and isotopic compositions of iron in coal and municipal waste fly ash, Sci. Total Environ., 838, 155974, https://doi.org/10.1016/j.scitotenv.2022.155974, 2022.

Li, S., Zhang, B., Wu, D., Li, Z., Chu, S. Q., and Ding, X.: Magnetic particles unintentionally emitted from anthropogenic sources: Iron and steel plants, Environ. Sci. Technol. Lett., 8, 295–300, https://doi.org/10.1021/acs.estlett.1c00164, 2021.

Li, T., Zhang, Q., Wang, X., Peng, Y., Guan, X., and Mu, J.: Characteristics of secondary inorganic aerosols and contributions to PM2.5 pollution based on machine learning approach in Shandong Province, Environ. Pollut., 337, 122612, https://doi.org/10.1016/j.envpol.2023.122612, 2023.

Lin, G. Y., Chen, H. W., Chen, B. J., and Chen, S.: A machine learning model for predicting PM2.5 and nitrate concentrations based on long-term water-soluble inorganic salts datasets at a road site station, Chemosphere, 289, 133123, https://doi.org/10.1016/j.chemosphere.2021.133123, 2022.

Liu, T., Chan, A. W. H., and Abbatt, J. P.: Multiphase oxidation of sulfur dioxide in aerosol particles: Implications for sulfate formation in polluted environments, Environ. Sci. Technol., 55, 4227–4242, https://doi.org/10.1021/acs.est.0c06496, 2021.

https://doi.org/10.5194/egusphere-2026-1615
Preprint. Discussion started: 8 April 2026

Lundberg, S. M., and Lee, S.: A unified approach to interpreting model predictions, Adv. Neural Inf. Process. Syst., 30, 4768–4777, 2017.

Mackie, D. S., Boyd, P. W., Hunter, K. A., McTainsh, H: Simulating the cloud processing of iron in Australian dust: pH and dust concentration, Geophys. Res. Lett., 32, L06809, https://doi.org/10.1029/2004GL022122, 2005.

Mahowald, N. M., Engelstaedter, S., Luo, C., Sealy, A., Artaxo, P., and Beniterz-Nelson, C.: Atmospheric iron deposition: Global distribution, variability and human perturbations, Annu. Rev. Mar. Sci., 1, 245–278, https://doi.org/10.1146/annurev.marine.010908.163727, 2009.

Mahowald, N. M., Hamilton, D. S., Mackey, K. R. M., Moore, J. K., Baker, A. R., Scanza, R. A., and Zhang, Y.: Aerosol trace metal leaching and impacts on marine microorganisms, Nat. Commun., 9, 2614, https://doi.org/10.1038/s41467-018-04970-7, 2018.

Mead, C., Herckes, P., Majestic, B. J., and Anbar, A.: Source apportionment of aerosol iron in the marine environment using iron isotope analysis, Geophys. Res. Lett., 40, 5722–5727, https://doi.org/10.1002/2013GL057713, 2013.

Meidan, D., Li, Q., Cuevas, C. A., Doney, S. C., Fernandez, R. P., and van Herpen, M. M. J. W.: Evaluating the potential of iron-based interventions in methane reduction and climate mitigation, Environ. Res. Lett., 19, 054023, https://doi.org/10.1088/1748-9326/ad3d72, 2024.

Miyakawa, T., Ito, A., Zhu, C., Shimizu, A., Matsumoto, E., and Mizuno, Y.: Trace elements in PM2.5 aerosols in East Asian outflow in the spring of 2018: emission, transport, and source apportionment, Atmos. Chem. Phys., 23, 14609–14626, https://doi.org/10.5194/acp-23-14609-2023, 2023.

Oakes, M., Ingall, E. D., Lai, B., Shafer, M. M., Hays, M. D., and Liu, Z. G.: Iron solubility related to particle sulfur content in source emission and ambient fine particles, Environ. Sci. Technol., 46, 6637–6644, https://doi.org/10.1021/es300701c, 2012.

Oeste, F. D., de Richter, R., Ming, T., and Caillol, S.: Climate engineering by mimicking natural dust climate control: the iron salt aerosol method, Earth Syst. Dynam., 8, 1–54, https://doi.org/10.5194/esd-8-1-2017, 2017.

Olgun, N., Duggen, S., Croot, P. L., Delmelle, P., and Dietze, H.: Surface ocean iron fertilization: The role of airborne volcanic ash from subduction zone and hot spot volcanoes and related iron fluxes into the Pacific Ocean, Global Biogeochem. Cy., 36, GB4001, https://doi.org/10.1029/2009GB003761, 2011.

Peng, X., Xie, T. T., Tang, M. X., Cheng, Y., Peng, Y., and Wei, F.: Critical role of secondary organic aerosol in urban atmospheric visibility improvement identified by machine learning, Environ. Sci. Technol. Lett., 10, 976–982, https://doi.org/10.1021/acs.estlett.3c00084, 2023.

Perron, M. M. G., Proemse, B. C., Strzelec, M., Gault-Ringold, M., and Bowie, A.: Atmospheric inputs of volcanic iron around Heard and McDonald Islands, Southern ocean, Environ. Sci.: Atmos., 1, 508, https://doi.org/10.1039/D1EA00054C, 2021.

Rodriguez-Navarro, C., and di Lorenzo, F.: Mineralogy and physicochemical features of Saharan dust wet deposited in the Iberian Peninsula during an extreme red rain event, Atmos. Chem. Phys., 18, 10089–10122, https://doi.org/10.5194/acp-18-10089-2018, 2018.

Sakata, K., Kurisu, M., Takeichi, Y., Sakaguchi, A., Tanimoto, H., and Tamenori, Y.: Iron (Fe) speciation in size-fractionated aerosol particles in the Pacific Ocean: The role of organic complexation of Fe with humic-like substances in controlling Fe solubility, Atmos. Chem. Phys., 22, 9461–9482, https://doi.org/10.5194/acp-22-9461-2022, 2022.

Sakata, K., Sakaguchi, A., Yamakawa, Y., Miyamoto, C., and Kurisu, M.: Measurement report: Stoichiometry of dissolved iron and aluminum as an indicator of the factors controlling the fractional solubility of aerosol iron – results of the annual observations of size-fractionated aerosol particles in Japan, Atmos. Chem. Phys., 23, 9815–9836, https://doi.org/10.5194/acp-23-9815-2023, 2023.

Sakata, K., Takano, S., Matsuki, A., Takeichi, Y., Tanimoto, H., and Sakaguchi, A.: Atmospheric chemistry in East Asia determines the iron solubility of aerosol particles supplied to the North Pacific Ocean, Atmos. Chem. Phys., 25, 11087–11107, https://doi.org/10.5194/acp-25-11087-2025, 2025.

https://doi.org/10.5194/egusphere-2026-1615
Preprint. Discussion started: 8 April 2026

Schroth, A. W., Crusius, J., Sholkovitz, E. R., and Bostick, B.: Iron solubility driven by speciation in dust sources to the ocean, Nat. Geosci., 2, 337–340, https://doi.org/10.1038/ngeo501, 2009.

Sedwick, P. N., Sholkovitz, E. R., and Church, T.: Impact of anthropogenic combustion emissions on the fractional solubility of aerosol iron: Evidence from the Sargasso Sea, Geochem. Geophys. Geosyst., 8, Q10Q06, https://doi.org/10.1029/2007GC001586, 2007.

Seo, H., Kim, G: Anthropogenic iron invasion into the ocean: Results from the East Sea (Japan Sea), Environ. Sci. Technol., 57, 10745–10753, https://doi.org/10.1021/acs.est.3c01084, 2023.

Shah, V., Jacob, D. J., Moch, J. M., Wang, X., and Zhai, S.: Global modeling of cloud water acidity, precipitation acidity, and acid inputs to ecosystems, Atmos. Chem. Phys., 20, 12223–12245, https://doi.org/10.5194/acp-20-12223-2020, 2020.

Shelley, R. U., Landing, W. M., Ussher, S. J., and Planquette, H.: Regional trends in the fractional solubility of Fe and other metals from North Atlantic aerosols (GEOTRACES cruises GA01 and GA03) following a two-stage leach, Biogeosciences, 15, 2271–2288, https://doi.org/10.5194/bg-15-2271-2018, 2018.

Shi, J., Guan, Y., Gao, H., Yao, X., Wang, R., Zhang, D: Aerosol iron solubility speciation in the global marine atmosphere with machine learning, Environ. Sci. Technol., 56, 16453–16461, https://doi.org/10.1021/acs.est.2c05266, 2022.

Shi, Z. B., Woodhouse, M. T., Carslaw, K. S., Krom, M. D., Mann, G. W., and Baker, A. R.: Minor effect of physical size sorting on iron solubility of transported mineral dust, Atmos. Chem. Phys., 11, 8459–8469, https://doi.org/10.5194/acp-11-8459-2011, 2011.

Shiraiwa, M., Ueda, K., Pozzer, A., Lammel, G., Kampf, C. J., and Fushimi, A.: Aerosol health effects from molecular to global scales, Environ. Sci. Technol., 51, 13545–13567, https://doi.org/10.1021/acs.est.7b04417, 2017.

Sholkovitz, E. R., Sedwick, P. N., Church, T. M., Baker, A. R., and Powell, C.: Fractional solubility of aerosol iron: Synthesis of a global-scale data set, Geochim. Cosmochim. Ac., 89, 173–189, https://doi.org/10.1016/j.gca.2012.04.022, 2012.

Shupert, L. A., Ebbs, S. D., Lawrence, J., and Gibson, D. J.: Dissolution of copper and iron from automotive brake pad wear debris enhances growth and accumulation by the invasive macrophyte Salvinia molesta Mitchell, Chemosphere, 92, 45–51, https://doi.org/10.1016/j.chemosphere.2013.03.002, 2013.

Takahashi, Y., Higashi, M., Furukawa, T., Mitsunobu, S: Change of iron species and iron solubility in Asian dust during the long-range transport from western China to Japan, Atmos. Chem. Phys., 11, 11237–11252, https://doi.org/10.5194/acp-11-11237-2011, 2011.

Tao, M., Xu, Y., Gong, J., Liu, Q: Estimation of aerosol acidity at suburban site of Nanjing using machine learning method, J. Atmos. Chem., 79, 141–151, https://doi.org/10.1007/s10874-022-09433-4, 2022.

van Herpen, M. M. J. W., Li, Q., Saiz-Lopez, A., Liisberg, J. B., Röckmann, T., and Cuevas, C. A.: Photocatalytic chlorine atom production on mineral dust–sea spray aerosols over the North Atlantic, Proc. Natl. Acad. Sci. USA, 120, e2303974120, https://doi.org/10.1073/pnas.2303974120, 2023.

Zhang, H., Li, R., Huang, C., Li, X., Dong, S., Fu, W., et al.: Seasonal variation of aerosol iron solubility in coarse and fine particles at an inland city in northwestern China, Atmos. Chem. Phys., 23, 3543–3559, https://doi.org/10.5194/acp-23-3543-2023, 2023.

Zhu, Q., Liu, Y., Shao, T., Tang, Y: Transport of Asian aerosols to the Pacific Ocean, Atmos. Res., 234, 104735, https://doi.org/10.1016/j.atmosres.2019.104735, 2020.

Zhu, Y., Li, W., Wang, Y., Zhang, J., Liu, L., and Xu, L.: Sources and processes of iron aerosols in a megacity in Eastern China, Atmos. Chem. Phys., 22, 2191–2202, https://doi.org/10.5194/acp-22-2191-2022, 2022.